

**DEVELOPMENT OF DUAL REPLACEABLE-LINK
ECCENTRICALLY BRACED FRAMES USING EQUIVALENT ENERGY BASED
DESIGN PROCEDURE**

by

Jesse Eric Edward Neitsch

B.ASc., University of British Columbia, 2012

A THESIS SUBMITTED IN PARTIAL FULFILLMENT OF
THE REQUIREMENTS FOR THE DEGREE OF

MASTER OF APPLIED SCIENCE

in

THE FACULTY OF GRADUATE AND POSTDOCTORAL STUDIES
(Civil Engineering)

THE UNIVERSITY OF BRITISH COLUMBIA
(Vancouver)

May 2017

© Jesse Eric Edward Neitsch, 2017

Abstract

Conventional seismic force resisting systems (SFRSs) rely on the use of ductile design philosophy, where structural components are designed to undergo large inelastic deformations to dissipate the sudden surge of the earthquake energy. This design philosophy has shown to be very effective in preventing structural collapse. However, the extensive inelastic deformation usually leads to significant damage to the structural and non-structural components. Many earthquake reconnaissance reports show that this design philosophy typically leads to hefty financial losses. Eccentrically Braced Frames (EBFs) have been proven through testing and earthquakes to exhibit a high level of ductile behaviour. However, the damage of the link leads to hefty repair costs, which lead to the Replaceable-Link Eccentrically Braced Frame (REBF). A well-tuned link can control the response of the REBF, which provides the advantage for the REBF over an EBF. While the link is designed to yield, and deform, the rest of the REBF and gravity system are designed to remain elastic. This mechanism makes the link act as a fuse in the REBF system, which allows the structure to be more resilient towards earthquakes.

In this study, a novel seismic design methodology named the Equivalent Energy-Based Design Procedure (EEDP) was implemented for the seismic design of two REBFs operating in parallel, which is referred to as the Dual REBF (DREBF) system. The conventional Equivalent Static Force Procedure (ESFP) was also used to achieve an alternate, comparative model. The designs and the design procedures themselves were compared to highlight potential benefits of designing from an energy based perspective.

EEDP allows the designers to select different performance objectives at different shaking intensities, where the structure can be designed to achieve these objectives using simple hand calculations. More importantly, the design can be achieved without iteration. This study

demonstrated that the design procedure of one simple prototype building utilizing both the ESFP and EEDP philosophies. Their seismic responses have been analyzed using detailed numerical models developed using OpenSees. The results of the nonlinear dynamic analysis showed that the EEDP designed DREBF can achieve the target performance defined by the designer at different shaking intensities.

Preface

This dissertation is original, unpublished, independent work by the author of this thesis. The author is responsible for the literature review, model development and presentation of the results.

Table of Contents

| | |
|---|-------------|
| Abstract | ii |
| Preface | iv |
| Table of Contents | v |
| List of Tables | viii |
| List of Figures..... | ix |
| List of Symbols | xi |
| List of Abbreviations..... | xii |
| Acknowledgements..... | xiii |
| Dedication..... | xiv |
| Chapter 1: Introduction..... | 1 |
| 1.1 Literature Review | 2 |
| 1.1.1 Current Canadian Seismic Design of Buildings | 2 |
| 1.2 Performance Based Design | 3 |
| 1.2.1.1 Performance-Based Plastic Design | 6 |
| 1.3 Development of Eccentrically Braced Frames | 8 |
| 1.4 Development of Earthquake Resilient Design | 11 |
| 1.5 Scope and Objective of the research..... | 16 |
| 1.6 Organization of Thesis | 17 |
| Chapter 2: Design Approach | 18 |
| 2.1 Theory of Equivalent Energy-Based Design Procedure | 18 |
| 2.1.1 Define Performance Objectives | 20 |

| | |
|--|-----------|
| <i>Service Level Objectives</i> | 20 |
| <i>Design Base Level Objectives</i> | 21 |
| <i>Maximum Level Objectives</i> | 23 |
| 2.1.2 Design Primary and Secondary Systems | 24 |
| 2.1.3 Plastic Design of Yielding Members (Shear Links) | 25 |
| 2.1.4 Capacity Design..... | 26 |
| 2.2 Prototype Building..... | 27 |
| 2.3 ESFP – Specific Application..... | 29 |
| 2.3.1 ESFP Parameters | 29 |
| 2.3.2 Base Shear Distribution | 33 |
| 2.3.3 Link Sizing | 33 |
| 2.3.4 Capacity Design..... | 35 |
| 2.4 EEDP – Specific Application | 37 |
| 2.4.1 Plastic Design of Yielding Members (Shear Links) | 39 |
| 2.4.2 Capacity Design..... | 41 |
| 2.5 Summary of the Design | 43 |
| Chapter 3: Numerical Modelling..... | 44 |
| 3.1 Numerical Model Description..... | 44 |
| 3.2 Calibration..... | 46 |
| 3.2.1 Experimental Results | 47 |
| 3.2.2 Numerical Calibration Model Description..... | 47 |
| 3.2.3 Calibration Results..... | 48 |
| 3.3 Comparison of Design and Model Time Period..... | 50 |

| | |
|--|-----------|
| Chapter 4: Evaluation of Seismic Performance | 51 |
| 4.1 Ground Motions..... | 51 |
| 4.2 Nonlinear Static Analysis (Pushover)..... | 55 |
| 4.3 Non-Linear Time History Analysis | 56 |
| 4.4 Performance Based Engineering Evaluation..... | 60 |
| 4.5 NLTHA Conclusion..... | 62 |
| Chapter 5: Rehabilitation Design with EEDP | 63 |
| 5.1 Rehabilitation Example..... | 63 |
| 5.2 Rehabilitation Comparison..... | 65 |
| Chapter 6: Summary and Conclusions | 67 |
| 6.1 Summary | 67 |
| 6.2 Future Research Needs | 69 |
| Bibliography | 71 |
| Appendix A: Site & Building Description | 76 |
| Appendix B: Equivalent Static Force Procedure | 78 |
| Appendix B: Equivalent Energy Design Procedure..... | 81 |
| Appendix D: Rehab Calculations | 88 |

List of Tables

| | |
|--|----|
| Table 1. Parameters used for ESFP Design..... | 32 |
| Table 2. Force Distribution applied to ESFP model..... | 33 |
| Table 3. Link size and values | 35 |
| Table 4. ESFP Non-yielding for each frame | 36 |
| Table 5. Parameters used for EEDP Design..... | 38 |
| Table 6. EEDP Link Primary (top) and Secondary (bottom) sizes and values | 40 |
| Table 7. EEDP Non-yielding elements Primary (top) and Secondary (bottom) sizes | 42 |
| Table 8. Frame weight comparison of ESFP and EEDP models..... | 43 |
| Table 9. OpenSEES Steel02 material definition (values shown in kip & in)..... | 48 |
| Table 10. Comparison of design and model fundamental period | 50 |
| Table 11. List of ground motions used for analysis with EEDP model..... | 53 |
| Table 12. Pushover load distribution up height of structure | 55 |
| Table 13. EEDP & ESFP Average Link yielding progression. | 59 |

List of Figures

| | |
|---|----|
| Figure 1. Rainflow depiction of seismic energy a) During seismic shaking, b) At the end of seismic shaking (from Christopoulos et al. [5]) | 5 |
| Figure 2. EBF systems (From Bruneau [21]) | 9 |
| Figure 3. REBF systems using bolted link (From Mansour [26]) | 10 |
| Figure 4. REBF systems using bolted link in Richmond B.C. (2016) | 11 |
| Figure 5. LCF system (From Malakoutian [32]) | 13 |
| Figure 6. BRKBTMF system (From Yang [33]) | 14 |
| Figure 7. DREBF Controlled fused structural response | 15 |
| Figure 8. Representation of Equivalent Energy Balanced Concept | 19 |
| Figure 9. Vancouver specific $\gamma_a - \mu$ relation for SFRS with fundamental period, $T = 0.81s$ | 22 |
| Figure 10. Vancouver specific $\gamma_b - \mu$ relation for SFRS with fundamental period, $T = 0.81s$ | 23 |
| Figure 11. SFRS distribution | 24 |
| Figure 12. Kinematic method representation using 5-storey REBF frame | 26 |
| Figure 13. Typical prototype structure [37] (top) Isometric layout (bottom) Plan layout. | 28 |
| Figure 14. Vancouver Uniform Hazard spectrum with period of interest marked with “X” | 30 |
| Figure 15. Half bay schematic of static force equilibrium from lateral load on EBF | 34 |
| Figure 16. Elastic capacity design model using SAP2000. | 36 |
| Figure 17. Target spectra for design and ground motion scaling | 37 |
| Figure 18. Primary, Secondary and Total building design static response | 38 |
| Figure 19. EEDP half-bay column tree elastic capacity design model using restoring forces | 42 |

| | |
|--|----|
| Figure 20. Analytical Models: ESFP frame A&B (left) and EEDP Primary frame A (middle) Secondary frame B (Right)..... | 43 |
| Figure 21. EEDP OpenSees DREBF Model (same for ESFP, different sizes) | 45 |
| Figure 22. Calibration Experimental test and numerical overlay | 49 |
| Figure 23. Response spectra of scaled ground motions. | 54 |
| Figure 24. Pushover curves of ESFP and EEDP compared with the EEDP design curve | 56 |
| Figure 25. Median Roof Drift Ratio (RDR) comparison. | 57 |
| Figure 26. EEDP Link yielding progression..... | 58 |
| Figure 27. ESFP Link yielding progression. | 58 |
| Figure 28. EEDP Frame Element Demand-Capacity Ratio (DCR) at MCE Intensity..... | 59 |
| Figure 29. ESFP Frame Element Demand-Capacity Ratio (DCR) at MCE Intensity | 60 |
| Figure 30. MCE level Repair Cost CDF – (EEDP ‘small dash’, ESFP ‘large dash’)..... | 61 |
| Figure 31. Pushover results from existing, rehabilitation and total systems | 66 |
| Figure 32. Median RDR Results of Existing and Rehabilitated systems | 66 |

List of Symbols

| | | |
|------------|---|--|
| Δ_y | : | Primary Yield drift of ENLSDOF |
| Δ_p | : | Secondary Yield drift ratio of ENLSDOF |
| Δ_u | : | Ultimate drift ratio of ENLSDOF |
| T | : | Fundamental period of the structure |
| g | : | Gravitational constant |
| S_a | : | Spectral acceleration (in units of g) |
| μ | : | Structural ductility factor |
| R_d | : | Ductility reduction factor |
| R_o | : | Overstrength reduction factor |
| W | : | Seismic weight of the structure |
| θ_p | : | Plastic inter-story drift ratio |
| β_i | : | Normalized shear distribution with respect to top story shear |
| F_i | : | Normalized equivalent lateral force at i^{th} storey |
| C_0 | : | MDOF displacement modification factor |
| γ_a | : | Energy modification factor of NLSDOF from Δ_y to Δ_p |
| γ_b | : | Energy modification factor of NLSDOF from Δ_p to Δ_u |
| V_{PR} | : | Distributed base shear of primary SFRS |
| V_{SE} | : | Distributed base shear of secondary SFRS |

List of Abbreviations

| | | |
|---------|---|---|
| REBF | : | Replaceable-Link Eccentrically braced frame |
| SFRS | : | Seismic force resisting system |
| MRF | : | Moment resisting frame |
| EBF | : | Eccentrically braced frame |
| PBPD | : | Performance-based plastic design |
| EEDP | : | Equivalent energy-based design procedure |
| ELSDOF | : | Elastic- single degree of freedom |
| ENLSDOF | : | Nonlinear- single degree of freedom |
| MDOF | : | Multiple degree of freedom |
| PBEE | : | Performance-based earthquake engineering |

Acknowledgements

It is people like professor Tony Yang who bring the heart in the engineering field to push the boundaries of convention. Thank you, professor for showing me that new design does not mean re-invention, but re-orientation. We can use the tools we already have to provide new outcomes, and in particular make cities more resilient to disastrous events. In turn, I must also acknowledge Dorian Tung, as a source of patience and practical guidance in working out with me the numerous issues in this research. It was evident, during this research process, how difficult it is to implement change and make technical progress practical. My admiration goes to those researchers who have found a way to bring successful, good change to a society that is ever in need.

Dedication

This thesis is dedicated to the true engineer, Jesus Christ, who is always with me, always inspires me, and has given me family, friends and housemates whom I am happily indebted to for their relentless support.

Chapter 1: Introduction

Recent earthquakes in New Zealand and Japan show that even countries with modern building codes are vulnerable to earthquakes, where structures might suffer significant damages with hefty financial and social losses. The primary reason for such losses lies in the process for seismic design of buildings. In most building codes, the buildings are designed to prevent collapse during a strong earthquake shaking. Despite that most well designed buildings have reached good collapse prevention performance objective, buildings may need significant rehabilitation and in some cases required demolition after an earthquake. This phenomenon is particularly obvious in the Christchurch region in New Zealand during the 2011 Christchurch earthquake. Elwood [1] presents that the region experienced significant building damages estimated over \$20 billion NZ dollars, with shut down the central business district region in downtown Christchurch city. Events like this reveal how resilient structures that can endure earthquakes with rapid repair are necessary in high earthquake zones.

Currently, most seismic design codes do not explicitly consider the damage and usability of a building after an earthquake. To address these concerns, new resilient seismic force resisting systems (SFRS) have been developed. The resilient SFRS uses structural fuses to dissipate the earthquake energy. After the earthquake these structural fuses can then be repaired or replaced efficiently. Hence, the structure can be functional immediately after the earthquake. This allows the structure to be resilient. In this thesis, a novel fused SFRS named the Dual Replaceable-Link Eccentrically Braced Frame (DREBF) is proposed. To ensure that the DREBF can be easily used by an engineer, a novel design procedure named Equivalent Energy-Based Design Procedure (EEDP) was adopted and derived to design the DREBF.

1.1 Literature Review

This section presents the literature review of existing seismic design procedure in Canada, new performance-based design procedure in seismic design and new innovative seismic fuse systems.

1.1.1 Current Canadian Seismic Design of Buildings

In Canada, buildings are designed using National Building Code of Canada (NBCC). Within NBCC 2015 Cl. 4.1.8.7, there are 2 procedures to design seismic force-resisting system. The design procedures are: 1) Equivalent static force procedure (ESFP); and 2) Dynamic Analysis. Between the two procedures, ESFP is the most commonly used. ESFP follows the concept that the structure can be treated as a Single Degree of Freedom (SDOF) system, where the base shear can be calculated using the mass multiplied by the acceleration experienced by the SDOF system. Depending on the damping inherent within the structure, the peak acceleration of the SDOF can be changed. The base shear is distributed up the building, where then the members of each storey can be sized to resist the earthquake and gravity forces. After the members have been designed, the deflection are then checked to ensure the deflection meets the limits specified by the building code standards. In many cases, the members have been sized for strength, must be resized to meet the deflection limits, which in turn changes the stiffness and demand on the structure, revealing the iterative nature of ESFP.

Equation 1 shows the minimum lateral earthquake force (base shear), V , specified by NBCC 2015 [2]:

$$V = \frac{S(T_a)M_v I_E W}{R_d R_o} \quad (1)$$

Where,

- i) I_E - The earthquake importance factor, specified in Table 4.1.8.5 of NBCC 2015 (0.9 low, 1.0 normal, 1.25 high, and 1.5 post disaster)
- ii) R_d - The ductility factor, specified in Table 4.1.8.9 of NBCC 2015 (1.0 – 5.0); 1.0 signifying an SFRS that has effectively no ductile failure mechanisms and 5.0 signifying an SFRS that fail in a high ductile manner.
- iii) R_o - The overstrength factor, specified in Table 4.1.8.9 of NBCC 2015 (1.0 – 1.5)
- iv) W - The total seismic weight of the building can be taken as the total dead load of the structure plus 25% of the design snow load.
- v) $S(T_a)$ – The spectral acceleration attributed to the building based on its period and the design spectrum for the region.
- vi) M_v - The Higher Mode Effect Factor, from Table 4.1.8.11 of NBCC 2015. Note That this factor accounts for the contribution of higher modes; it would be unconservative if the shear force demand was based solely on the acceleration induced by the first mode.

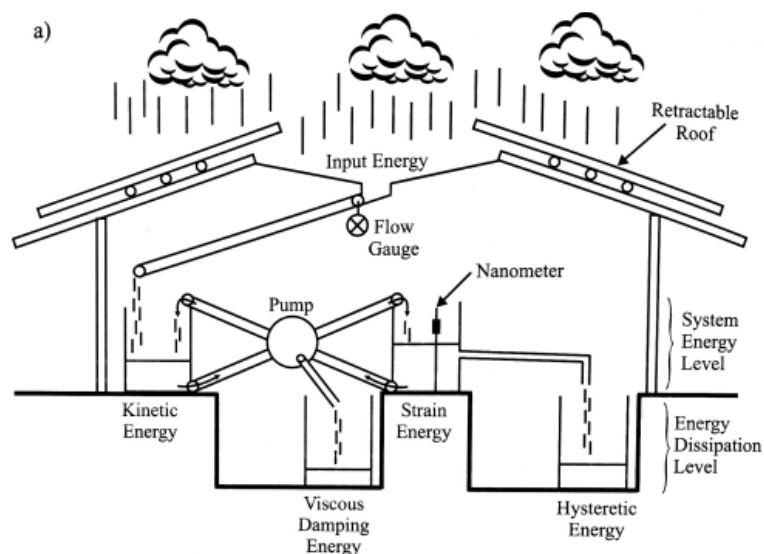
To ensure the structure designed using ESFP does not collapse, Cl. 4.1.8.13 of NBCC 2015 states the inelastic drift limits of 1.0%, 2.0% and 2.5%, are selected for post disaster, high and all other buildings, respectively. If the structure does not meet this drift limit, the members of the SFRS need to be stiffened until drift compliance is achieved. This process reveals that drift may control the design indirectly, which may cause the design to be iterative.

1.1.2 Performance Based Design

As presented in the ESFP, the strength and stiffness of the structure are not necessary related. Different failure modes in the structure could result in different performance of the structure.

Priestly notes that the plastic hinges formed in beams prior to columns leads to a more robust failure mechanism and indicates that the performance of the building is effectively dependent on the design process [3]. The Equivalent Energy-based Design Procedure (EEDP) is a Performance Based Design (PBD) procedure that seeks to design for stiffness and strength at the beginning of the design phase. EEDP uses the energy-balanced concept and plastic design procedures to design the structure to achieve the strength and stiffness at the same time without iteration.

Energy design is of specific interest to SFERS designers, as energy calculations are scalar in nature and tend to make for less complicated calculations as compared with force-vector calculations. In the 1950's Housner [4] introduced his observation of applying an energy balanced concept to seismic design. He showed that seismic energy is a stable value that is transformed in the structural response between kinetic, strain, inherent damping and hysteretic damping energies, where kinetic energy is at a minimum when strain energy is at a maximum. The sum of these four energies at any point should equal the energy input into the structure by the earthquake. A visualization of the energy transformation is presented in by Christopoulos et al. [5] that uses a building which receives a rain fall, as shown in Figure 1.



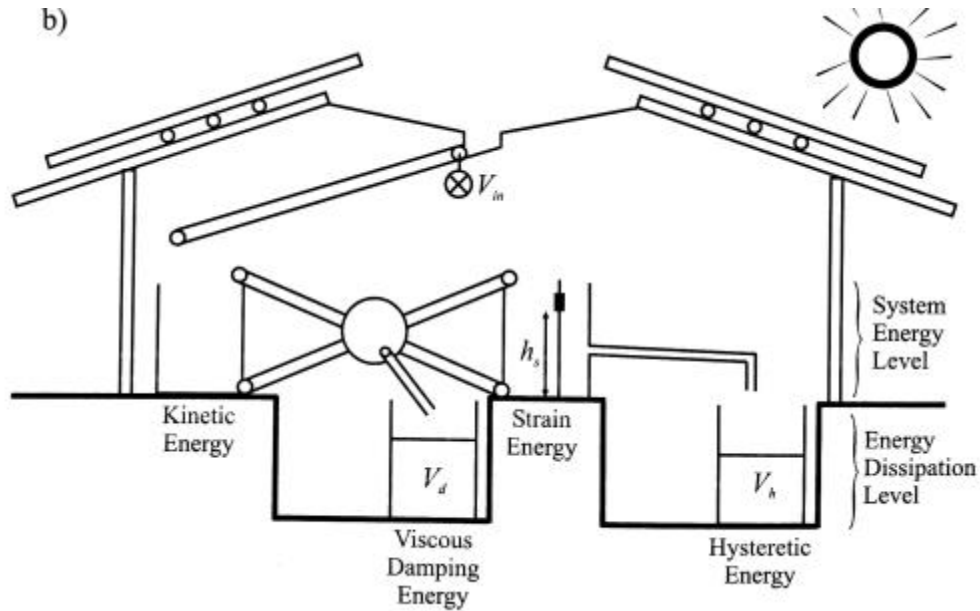


Figure 1. Rainflow depiction of seismic energy a) During seismic shaking, b) At the end of seismic shaking (from Christopoulos et al. [5])

The building collects the rain, which is the earthquake input energy, and contains the water in a basin representing the kinetic energy. The kinetic basin “pumps” the water into a strain basin, which has a water level regulated by an indicator, which represents elemental yield strength or strain, that empties water at a certain level. Below that level water leaves the basin via another “pump” into the kinetic basin. The water is essentially pumped back and forth between the kinetic and strain basins until no water is left. Water leaves the system by losses in the pump, which symbolizes inherent damping energy dissipation in the structure and when the strain basin exceeds its limit, symbolizing hysteretic damping energy dissipation. The sooner all the water can exit the system, the sooner motion will end and static equilibrium will be accomplished.

Akiyama [6]–[8] agreed with the observation presented by Housner. He echoed that earthquake energy is a stable value that can be calculated, depending on the mass and fundamental period of the structure. The energy concept was further developed by Fischinger [9] who explained

that the kinetic energy of the system tends to change into total strain energy (elastic and hysteretic), and energy dissipated through inherent damping, which is congruent with the visualization given in Figure 1. If the damping is neglected, the input earthquake energy can be approximated by the total strain energy of the system. The total strain energy is broken into elastic strain stored in the members and hysteretic strain energy absorbed by yielding members (see strain basin in Figure 1). Taking the concepts of energy design, Goel and Chao [10]–[13] introduced a Performance Based Plastic Design (PBPD) procedure that is prescriptive in nature and not cumbersome in practice.

1.1.2.1 Performance-Based Plastic Design

The purpose behind plastic design is to account for and utilize hysteretic energy potential of structural members by considering their inelastic response. If not properly accounted for, this inelastic response can produce major deflections in structural elements potentially causing severe damage, and even collapse by exceeding the drift capacity of the gravity system. Due to the potential complexity and variety of failure mechanisms inherent in structures with numerous degrees of freedom, having a blanket elastic drift limit, as proposed by ESFP, for design can potentially miss critical scenarios that cause excessive structural damage. Plastic design becomes more relevant when considering the control of these excessive drifts. Goel and Chao [13] have developed PBPD, a design method that considers both the strength and drift performance of a structure using the plastic mechanisms formed in a structure during an earthquake. PBPD directly designs the structure to achieve main performance objectives through plastic mechanisms.

Three major steps are considered in this design procedure; calculation of design base shear, distribution of base shear up the structure and capacity design of non-yielding elements. The three steps are briefly described in the following:

Design Base Shear

Design base shears are developed for a given hazard level by taking the work-energy needed to monotonically push an Elastic Linear Single Degree of Freedom (ELSDOF) structure to a desired drift and equating it to the energy absorbed by an Elastic Non-Linear Single Degree of Freedom (ENLSDOF) system. The equation to calculate the base shear uses an energy modification factor, γ , that is dependent on the structural ductility and ductility reduction factors proposed by Newmark and Hall [14].

$$\frac{V_y}{W} = \frac{-\alpha + \sqrt{\alpha^2 + 4\gamma S_a^2}}{2} \quad (2)$$

Where V_y is the yield strength of the SFRS selected and W , the seismic weight of the structure. The spectral acceleration, S_a , is defined on the design hazard selected and α is a dimensionless parameter based on the plastic component of the target drift and the building period.

Base Shear Distribution

These base shears are then distributed up the structure based on relative distribution of maximum storey shears noted during a number of non-linear dynamic analyses. The formula used to distribute the base shear up the building is given as follows:

$$F_i = (\beta_i - \beta_{i+1}) \left(\frac{w_n h_n}{\sum_{j=1}^n w_j h_j} \right)^{0.75T^{-0.2}} V_y \quad (3)$$

Where β_i is the ratio of the current story shear, V_i to the roof shear V_n .

Design of Non-Yielding Members

The members that need to be protected, such as the gravity system, need to remain elastic during an earthquake. This is accomplished by capacity designing the non-yielding members of the SFRS

such that they can resist the plastic and overstrength capacity induced by the yielding members. Typical elastic analysis can accomplish this, however a ‘column tree’ approach is given by Goel and Chao that incorporates a stabilizing force related to the base shear distribution and plastic mechanism as well as P-Delta effects.

Goel and Chao report that this method has been successfully applied to steel moment frames, buckling restrained brace frames and eccentrically braced frames. Because the method is based on target structural drifts and plastic mechanisms in the SFRS, there is no need for reduction factors, such as R_d and R_o . The plastic mechanism is specifically designed to be the only location in the structure that experiences yielding during seismic activity, and therefore, the members outside of this region must be designed to stay elastic during loading and yielding. This is a capacity design approach, which ensures the performance of the structure is met by “forcing” or activating the desired plastic mechanism in the structure.

Contrasted to ESFP, which is notorious for its many iterations in design, PBPD no iteration as drift and strength targets are considered at the beginning of design. Non-linear analysis has confirmed that this method achieves the objectives and does so without iteration, showing that movement toward a more controlled building response is capable by the designer. However, both ESFP and PBPD can only design a building for a single hazard. EEDP takes the ideals and process from energy and plastic design as the basis for the design procedure and enables the SFRS design to multiple hazards.

1.1.3 Development of Eccentrically Braced Frames

EBFs are a highly efficient SFRS and have been proven through testing and earthquakes to exhibit a high level of ductile behaviour. Figure 2 shows different configurations of EBFs. The

link (hatched portion) is designed to provide the stiffness and strength needed to dissipate the earthquake energy. The link section, length and size can be manipulated to regulate structural stiffness of the SFRS and used to match desired drift ratios. Bosco et al. [15] and Shen et al. [16] show that the material properties such as kinematic and isotropic hardening play an important role in the non-linear behaviour of the link which determines energy dissipation of the SFRS [15–20]. Energy is dissipated in the link through its stable hysteretic response to cyclic loading. While the link is designed to yield and deform, the rest of the SFRS and gravity system is designed to remain elastic [15]. This mechanism regulates damage propagation; by experiencing damage itself, it absorbs the damage of neighboring elements keeping them in an elastic state. This is the fundamental ideal of a structural fuse.

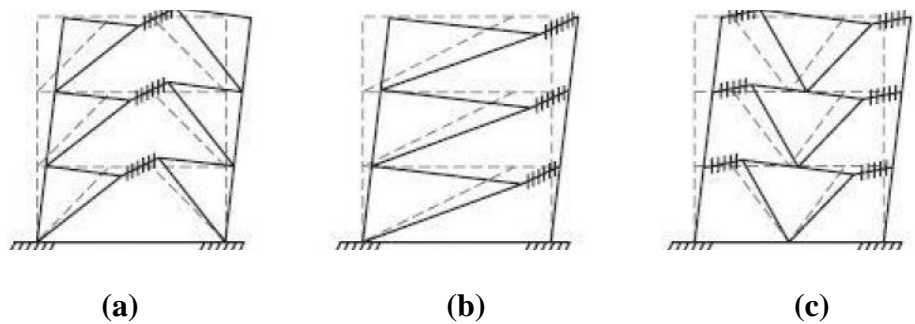


Figure 2. EBF systems (From Bruneau [21])

Conventionally, EBFs are designed having the beam and link section as a single continuous link member. Clifton [22] et al. report that during the Christchurch earthquake in 2011, the links of EBF structures sustained damage while operating in a ductile manner. Though this is a desirable result, repair of the entire beam is invasive and costly. In pursuit of resilience, Replaceable-Link Eccentrically Braced Frames (REBF) have been introduced [16, 23–26]. An REBF uses a link that is moment-connected to the outside beam, ideally via bolt connections making ease of replacement. This usually results in the use of a link that is smaller than the beams. In this system, the replaceable link acts as a structural fuse, which engages at forces larger than the link yield

capacity. The link is designed to operate primarily in shear and bending, and to be decoupled from the gravity system as well as contribute low axial resistance.

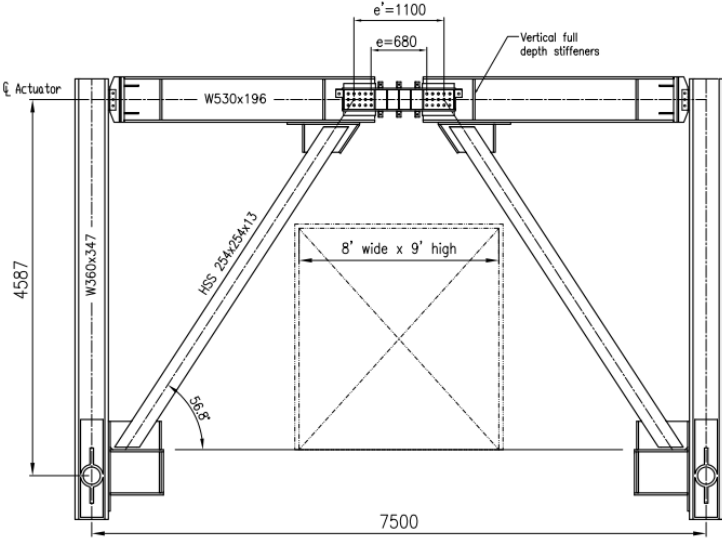


Figure 3. REBF systems using bolted link (From Mansour [26])

Figure 3 shows the REBF configuration used by Mansour in his investigation of the uses of replaceable links in EBFs. His thesis revealed that the REBF was able of achieving a ductile, stable mechanism during earthquake shaking even with conventional flooring attached along the top of the frame. These results encourage the progression of resilient structures and reveal that such an ideal can be attained with an REBF.



Figure 4. REBF systems using bolted link in Richmond B.C. (2016)

Figure 4 shows an REBF that has been built to the current code standards and detailed according to S16-09 [27] for replaceable links. Note again the different size in link and beams and the current interest in construction to use these systems.

1.2 Development of Earthquake Resilient Design

Designing for performance which considers the drifts of the structure as well as the strength enables the designer to take control of the state of the structure at any given time of its life cycle. Resilient structures are ones that can endure a variety of events by responding uniquely to each event. Resiliency is shown in the structure's ability to maintain the design state for a given event. EEDP works on this philosophy by providing a design method for structures that use fuses. A fuse can be tuned to damage at a specified load and begin to dissipate energy in a damaged state. In fuse structures, the non-fuse elements are designed for one quantifiable elastic state, and intended

to remain elastic, whereas the fuse is designed for a minimum of two quantifiable states and predictable behaviour in the inelastic range.

EEDP was developed considering that regions of high seismicity can experience ground shaking of different intensities. The different intensities have proven to be trouble to design for when using the static technique which can only employ a safe design by considering the maximum earthquake intensity. Which is again related to the fact that ESFP gives a design based on the elastic state of the members.

EEDP is intended to fill the holes in design that the static procedure cannot account for, for example; where drift sensitive design is required, drift is directly considered at the beginning of design, not checked for at the end of the design as is done in ESFP. Multiple levels of earthquakes can be considered with EEDP by designing tuned, fused systems that have controllable inelastic design states shown in Figure 7. Iteration in the design phase is avoided as the major targets are accounted for in the beginning of design. Uncertainty is further reduced as there are no need for general factors such as R_d and R_o which were introduced in ESFP.

Two examples of fused structural systems that can be designed using EEDP are given in the following paragraphs. The purpose of these systems is to improve the structural performance during an earthquake and control the state of the structure after the earthquake. The structural fuses are designed to dissipate the sudden surge of earthquake energy while protecting the remaining structure [23], [28]–[31]. The tri-linear response shown in Figure 7 also enables these systems to achieve specific performance at different earthquake intensities.

- Linked Column Frame (LCF)

The LCF utilizes two systems to control seismic performance: moment frame connected with a linked column. The two systems work in parallel where the linked column is designed to yield at lower structural drifts than the moment frame.

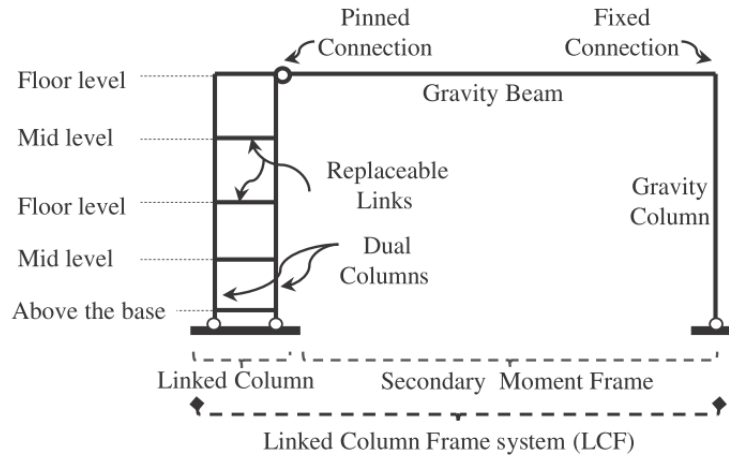


Figure 5. LCF system (From Malakoutian [32])

The links are the fuse in the system, designed to dissipate energy while protecting the moment frame and be replaceable after an earthquake. Malakoutian and Dusicka et al. [23], [32], [29] give a description of the seismic performance of the LCF and Figure 5 as a depiction of the system in a building.

- Buckling Restrained Knee Braced Truss Moment Frame (BRKBTMF)

Industrial buildings often use open web steel joists (OWSJ) in construction for the sake of achieving large spans. A buckling restrained brace, as self-explained, is a brace that is inhibited from buckling, ensuring that the brace yields in tension and compression. The two structural systems are combined in the BRKBTMF.

The truss and columns are designed to remain elastic while the Buckling Restrained Knee Braces (BRKBs) are located at the junction of the truss and column as shown in Figure 6. At lower

drifts the BRKBs are designed to yield, as a fuse and dissipate energy, shielding the moment frame created by the truss-column connection.

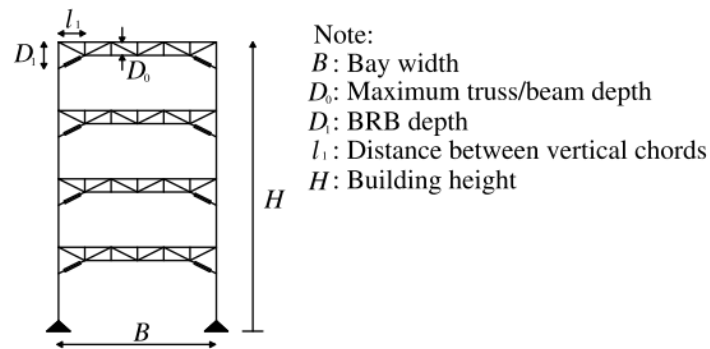


Figure 6. BRKBTMF system (From Yang [33])

The BRKBs provide stable yielding in both tension and compression and are easily replaced, hence why they are designed to yield first.

Both of these systems, the LCF and BRKBTMFT, can be designed for multiple hazards. However, both systems are relatively new to industry, therefore, this thesis presents another system that seeks to continue the development of the familiar EBF as noted in section 1.3. The Dual Replaceable-Link Eccentrically Braced Frame (DREBF) is the fused system presented in this thesis, shown in Figure 7. The DREBF is two Replaceable-Link Eccentrically Braced Frames (REBFs) that operate in parallel with one another, separated by a bay but linked by the diaphragm. The system can be designed for multiple hazards using EEDP. Having the two systems work coincidentally provides the ability for the SFRS to have a tri-linear pushover response, see Figure 7, depending on the strength and stiffness of each system. The tri-linear response gives the system the ability to perform specifically at different earthquake intensities.

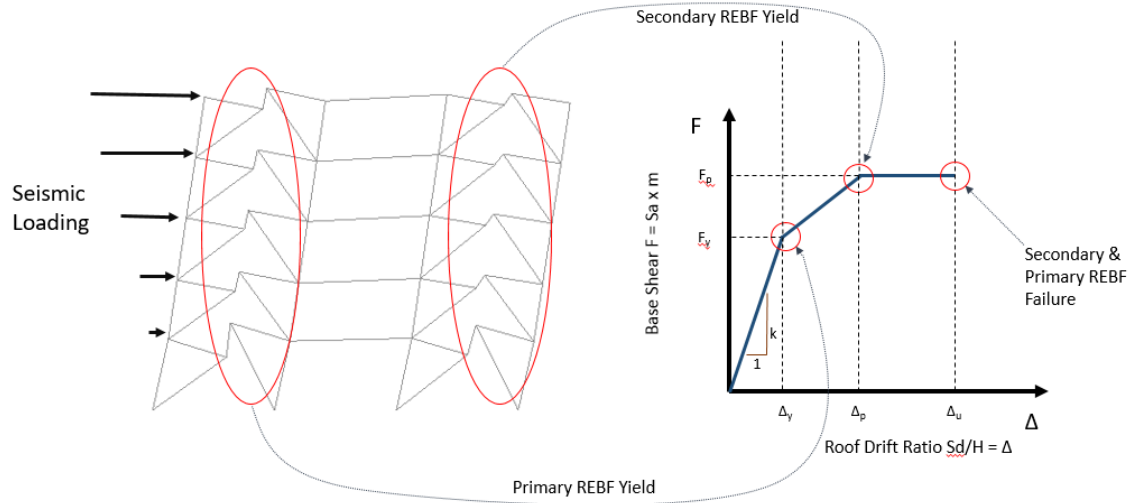


Figure 7. DREBF Controlled fused structural response

Again, the value of this system is found in the close tie it has with conventional EBF link detailing standards and how familiar the construction industry is with EBFs. The fuses in this system are found in the two separate frames as the link beams connecting the braces. One frame is designed to have the links yield at lower drifts than the second. The links yield to dissipate energy and shield the braces and gravity system from damage. These links can be easily inspected, repaired or replaced without affecting the functionality of the structure. EEDP and fused structures give designers now the opportunity to solve the economic problem inherent with the undefined post-earthquake state of a structure.

1.3 Scope and Objective of the research

Considering the need for more resilient structures in communities, this research focusses on the use of EEDP in the design of a DREBF for use by practicing engineers in Canada. The following sections show the scope and objective of the research:

- (i) Develop EEDP design of DREBF.
- (ii) Design DREBF using EEDP and compare the design with ESFP.
- (iii) Develop robust numerical models of DREBF.
- (iv) Perform non-linear dynamic analyses on the numerical models to evaluate the seismic performance of the DREBF.
- (v) Use performance based evaluation method to evaluate seismic performance of the DREBF.
- (vi) Apply EEDP for rehabilitation.

1.4 Organization of Thesis

This thesis is divided into the following six chapters:

Chapter 1 provides the brief introduction to summarize the motivation and literature of the research.

Chapter 2 introduces the design approaches developed for the DREBF. In addition, a prototype building was designed using EEDP and ESFP presented in this chapter.

Chapter 3 presents the detailed numerical modelling approach for the DREBF.

Chapter 4 presents the results of the seismic assessment of the DREBF. The results are discussed and compared to draw relevant design implications. PBEE was used to give more insight to the results.

Chapter 5 explores how EEDP can be used in rehabilitation design of existing structures.

Chapter 6 discusses and presents the summary of findings, future work, and implications for the practical design in industry.

Chapter 2: Design Approach

This chapter presents the fundamental approach to applying EEDP to a structure. Initially, discussion is made regarding the general application of EEDP. A building is then presented as a prototype for design. Both ESFP and EEDP are applied to the building to arrive at specific design models. Section 1.1.1 gives the steps of ESFP. Section 2.1 gives an overview of the application of EEDP. Section 2.2 shows the information of the prototype building. Section 2.3 presents the application of ESFP to design the prototype building. Section 2.4 presents the application of EEDP to design the prototype building.

2.1 Theory of Equivalent Energy-Based Design Procedure

This section gives an overview of the theory and general application of EEDP. As noted in section 1.1.2, EEDP is developed from the ideals presented in energy design and combines practical techniques taken from PBPD. EEDP seeks to improve upon PBPD by proposing a prescriptive method to design an SFRS for multiple hazard levels. The theory and application of EEDP is presented comprehensively by Yang et al. [34]–[36] for the sake of designing fused structural systems. The method is non-iterative and designs for drift targets related to the seismic hazard associated with the building location. Figure 8 presents the concept of EEDP. The area under Elastic Linear Single Degree of Freedom (ELSDOF) curve represents the strain energy transferred to the building from an earthquake. The area under the Elastic Non-Linear Single Degree of Freedom (ENLSDOF) curve represents the strain energy stored in the structure which is less than the ELSDOF due to the energy dissipated from fuses yielding. The ENLSDOF, which represents the real response of the SFRS, has three design states. The energy for each design state

is presented as ΔE_e , ΔE_{NM1} , ΔE_{NM2} , which are taken as elastic, primary inelastic and secondary inelastic states. Under Service Level Earthquakes (SLE), the SFRS will remain elastic, under Design Base Earthquakes (DBE) the structure will operate in the primary inelastic range and under the Maximum Credible Earthquake (MCE) the structure will operate in the secondary inelastic range. This concept of energy transformation is used to design an SFRS that has a tri-linear backbone response which operates differently depending on the hazard. The energy transformation is further explained in the general application of EEDP.

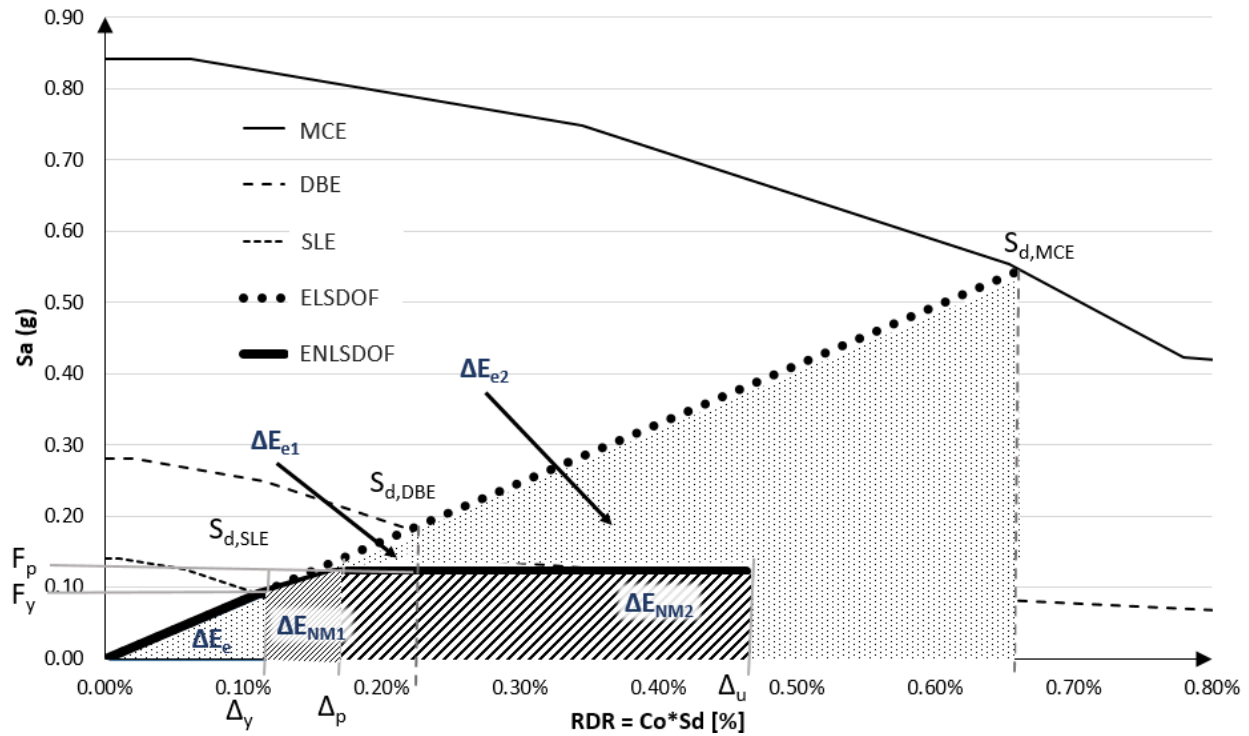


Figure 8. Representation of Equivalent Energy Balanced Concept

EEDP is used to size specific yielding elements, structural fuses, of an SFRS. Capacity design techniques are further employed to develop the full model. The general steps for application are:

- Define performance objectives (design ground motion spectra and displacement targets to define tri-linear response)
- Define response of primary and secondary systems (break down the tri-linear response to define the different inelastic responses of each system)
- Plastic design of the fuses to achieve the desired responses
- Capacity design of frame elements outside of the fuses

2.1.1 Define Performance Objectives

The power of EEDP is directly realized in its ability to set up performance targets which are defined by the designer and owner collaboration. EEDP uses three levels of shaking intensities to define the performance objectives, given in increasing intensity: Service Level Earthquake (SLE), Design Base Earthquake (DBE), and Maximum Credible Earthquake (MCE). Typically, the three different intensities are defined by starting with the expected seismic hazard of the area and scaling that spectrum up or down to define the other two spectrums.

Service Level Objectives

Under the SLE, the system is designed to remain elastic. Four base variables comprise the SLE level; the initial yield displacement, Δ_y , The SLE spectrum, the fundamental building period, T , and the base shear at which the initial yield displacement occurs, F_y . Figure 8 shows the definition of these initial parameters. Because these four variables are dependent on each other, only two of the four can be exclusively chosen, and the other two are calculated from the first. For example, to have a building with a specified period and specified yield strength, both the spectral acceleration and spectral displacement values will be directly dependent on those variables and so

forth when choosing any pair of the four mentioned variables. The variables are dependent on one another shown in the following equations, where $S_{a,y}$ is the spectral acceleration defined by the intersection of the Single Degree-of-Freedom (SDOF) spectrum with specified period on the S_a vs. S_d plot (Figure 8):

$$F_y = m(S_a)_{SLE} \quad (4)$$

$$\Delta_y = C_o(S_d)_{SLE}/H \quad (5)$$

$$T = 2\pi \sqrt{\frac{S_d}{S_a}} = 2\pi \sqrt{\frac{m \Delta_y}{C_o F_y}} \quad (6)$$

Design Base Level Objectives

The transition between the SLE and DBE level of shaking is represented by the primary SFRS yielding. EEDP uses the yielded replaceable link in the primary SFRS to dissipate energy at this level and shield the secondary system and gravity elements from the increasing intensity. Upon reaching the DBE level, the secondary SFRS is designed to yield, increasing the system's energy dissipation capacity. At this level, the variables that need to be defined are the ultimate base shear strength, F_p , and the roof displacement at which this force occurs, Δ_p . Each variable is dependent on each other, so only one can be chosen. The calculation is given for each as such:

$$F_p = \frac{2\Delta E_{e1}}{\gamma_d(\Delta_p - \Delta_y)} - F_y \quad (7)$$

$$\Delta_p = C_o(S_d)_{DBE}/H \quad (8)$$

Figure 8 shows how these variables interact to define the tri-linear backbone response of the structure. After the primary system yields, the structure departs from the ELSDOF response and softens, elongating the period. This transition is quantified by the first energy transformation

factor, γ_a . The purpose of this variable is to take the elastic strain energy developed by the ELSDOF and convert it to the strain energy experienced by the ENLSDOF, thereby accounting for the energy dissipated from the first yielded system. The change of energy between the SLE and DBE levels is taken as ΔE_{e1} and the corresponding non-linear strain energy experienced by the structure is taken as ΔE_{NM1} . The energy transformation factor, γ_a is calculated based on a series of Nonlinear Time History Analyses (NLTHA), further explained by Yang et al. [35] and is related to the ductility (Δ_p / Δ_y) and fundamental period of the structure, as shown in Figure 9.

$$\Delta E_{e1} = \frac{mC_o}{2} [(S_a)_{DBE} + (S_a)_{SLE}] [(S_d)_{DBE} - (S_d)_{SLE}] \quad (9)$$

$$\Delta E_{NM1} = \frac{mH}{2} [(S_a)_p + (S_a)_y] (\Delta_p - \Delta_y) \quad (10)$$

$$\Delta E_{e1} = \gamma_a \Delta E_{NM1} \quad (11)$$

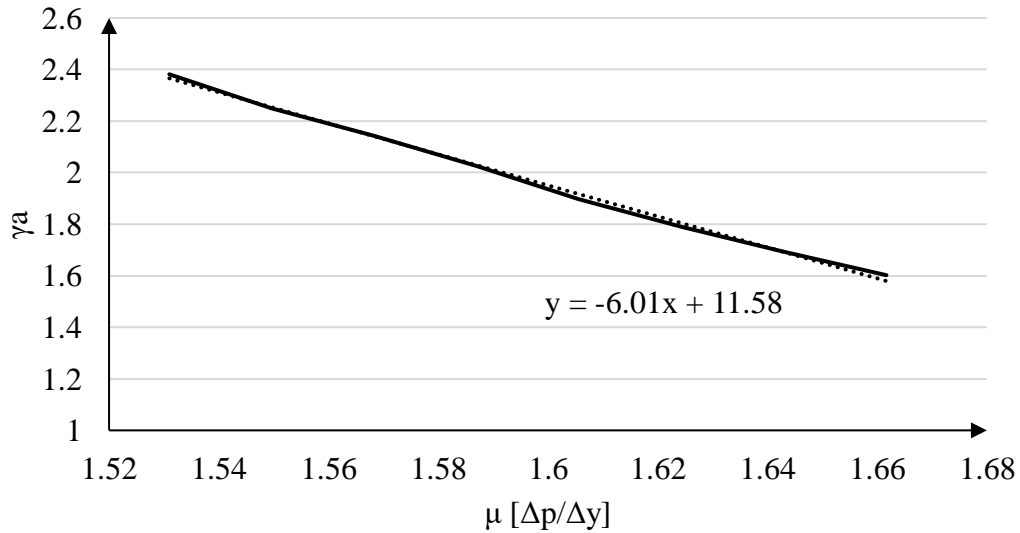


Figure 9. Vancouver specific γ_a - μ relation for SFRS with fundamental period, $T = 0.81s$.

Maximum Level Objectives

At the MCE level of shaking, both primary and secondary SFRSs have yielded and are designed to prevent collapse of the gravity system. This is done by translating the increased energy into a maximum displacement. Having the MCE defined initially, and the variables from the previous two sections defined, the maximum drift, Δ_u , can be calculated.

Like the previous level, the energy stored by the ELSDOF, ΔE_{e2} , structure must be transformed to anticipate the amount of energy dissipated by the yielding of both the primary and secondary SFRSs. The energy stored in the structure of the non-linear system, the ENLSDOF is taken as ΔE_{NM2} . The factor introduced at this stage to quantify the transformation is γ_b . The energy transformation factor γ_b is also calculated based on a series of NLTHAs and is related to the ductility (Δ_p / Δ_y) and fundamental period of the structure, as shown in Figure 10.

$$\Delta E_{e2} = \frac{mC_o}{2} [(S_a)_{MCE} + (S_a)_{DBE}] [(S_d)_{MCE} - (S_d)_{DBE}] \quad (12)$$

$$\Delta E_{NM2} = m(S_a)_p H(\Delta_u - \Delta_p) = F_p H(\Delta_u - \Delta_p) \quad (13)$$

$$\Delta E_{e2} = \gamma_b \Delta E_{NM2} \quad (14)$$

$$\Delta_u = \frac{\Delta E_{e2}}{\gamma_b F_p} + \Delta_p \quad (15)$$

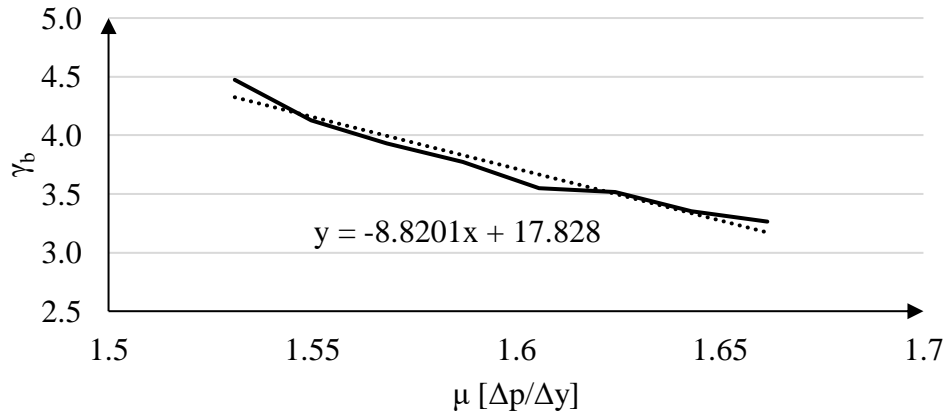


Figure 10. Vancouver specific γ_b - μ relation for SFRS with fundamental period, $T = 0.81$ s.

Figure 8 shows the interaction of the design states and the targets with their respective transformation energy.

2.1.2 Design Primary and Secondary Systems

The performance objectives in the previous section define a tri-linear backbone response comprised of two bi-linear systems working in parallel. To design the two systems the tri-linear curve is broken down as follows:

$$F_{PR} = F_y \frac{\mu_p - \lambda}{\mu_p - 1} \quad (16)$$

$$F_{SE} = F_y \mu_p \frac{\lambda - 1}{\mu_p - 1} \quad (17)$$

Where F_{PR} and F_{SE} are the yield strength of the primary and secondary SFRSs, respectively. Furthermore, λ is taken as the ratio of F_p to F_y and μ_p the ratio of Δ_p to Δ_y . Figure 11 below depicts this interaction and distribution. The case given in Figure 11 shows the primary system yielding at a lower strength and displacement than the secondary system. Different combinations of yield drift and yield strength of the total system can be achieved based on the preference of the designer.

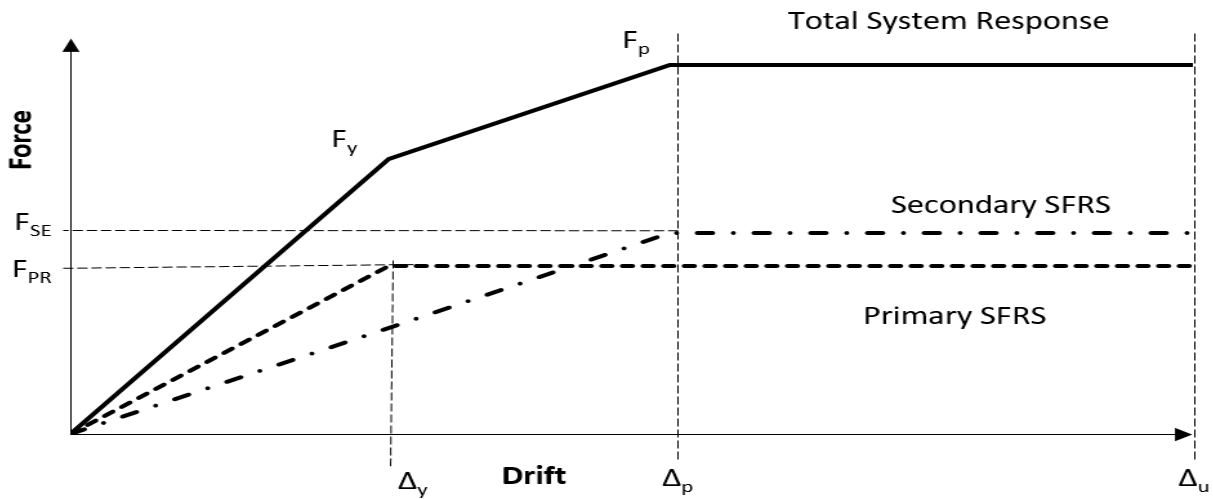


Figure 11. SFRS distribution

2.1.3 Plastic Design of Yielding Members (Shear Links)

The fuses in the DREBF system are designed in this step. A free-body diagram of the specific structure is used as well as the kinematic theory to determine the demand the links (fuses) will be designed for. The principles of work state that external energy (W_{ext}) working on the structure must be equivalent to the internal energy (W_{int}) expressed by the structure. In this case, the energy observed by the structure that causes the links to yield is quantified by the force at which each storey is subjected to, which is resisted by the link. The design storey force is quantified by distributing the design base shear up the building. The base shears to be distributed are those which correspond to the primary and secondary SFRSSs, F_{pr} and F_{se} respectively. The equation below presented by Goel & Chao shows how the base shear is distributed as storey shear, F_{pri} , or F_{sei} , to each level above the base (the primary base shear F_{pr} is shown, but the same process is used for the secondary base shear F_{se} as well).

$$F_{pri} = C_{vi}F_{pr}; \text{ shear at storey 'i'} \quad (18)$$

$$C_{vi} = (\beta_i - \beta_{i+1}) \left(\frac{w_n h_n}{\sum_{j=1}^n w_j h_j} \right)^{0.75T^{-0.2}} \quad (19)$$

$$\beta_i = \left(\frac{\sum_{j=1}^n w_j h_j}{w_n h_n} \right)^{0.75T^{-0.2}} \quad (20)$$

β is a factor developed by Goel and Chao used to represent the anticipated plastic behaviour of Multi Degree-of-Freedom (MDOF) systems and is the factor used to distribute the design shear force of each link to each storey.

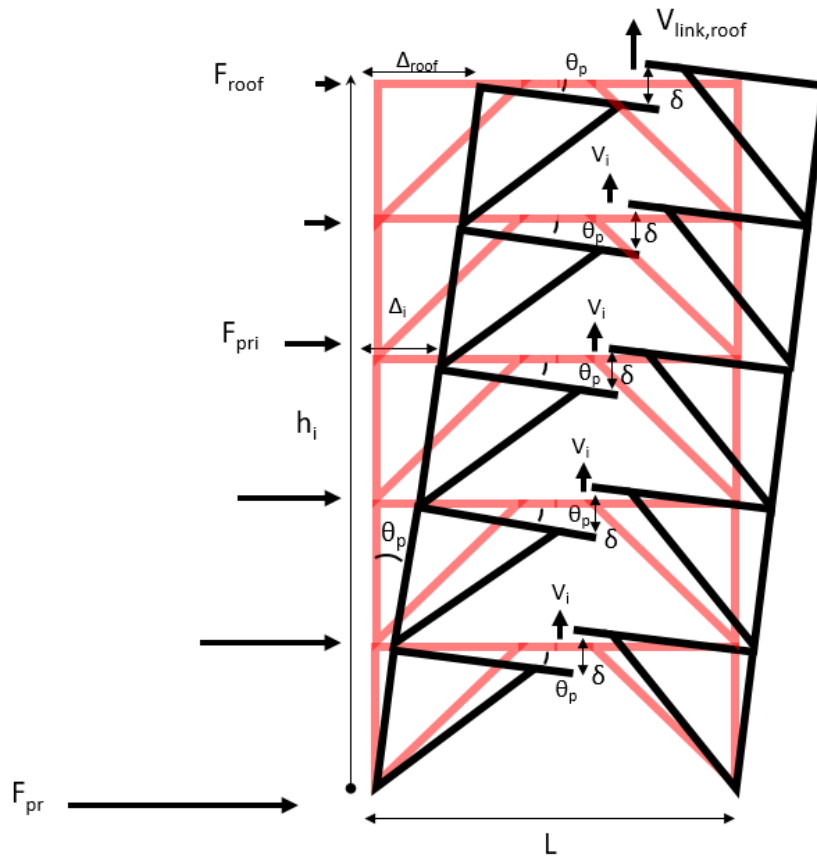


Figure 12. Kinematic method representation using 5-storey REBF frame

In the example above, having determined the design force for each link, V_i , it is possible to size them based on that shear demand.

2.1.4 Capacity Design

Similar to PBPD, the non-yielding elements must be designed to remain elastic during the earthquake. This implies that they must be able to resist the probable load induced by the yielding elements to which they are connected. Following PBPD, a column tree can be modelled in an elastic analysis where restoring forces are applied to each floor calculated based on the applied probable forces and gravity loads on each floor that induce a moment around the base.

2.2 Prototype Building

Figure 13 shows a prototype office building adapted from Murphy [37]. The prototype building was chosen to be located in Vancouver BC. The structure and layout are orthogonal to avoid both vertical and horizontal irregularities. The building is assumed to be built on soil classified as site class C. The hazard spectrum for Vancouver is presented in section 2.3.1. This design spectrum used for this building in both EEDP and ESFP design. The only irregularity that was adopted in the analysis was the heightening of the first storey to accommodate shops, as is custom for a new build development.

The SFRS employed in the structure is the REBF. Two REBFs are placed in each direction. The building has a total of five floors, each with a seismic weight 11583 kN except the roof, which has a seismic weight of 7299kN. The total building weight is 54687 kN. Similarly, each floor has a height of 3.65m with exception to the first floor which has a height of 4.25m. The total building height is 18.85m. Each bay is 9m wide, with brace bays as shown in plan. Each brace bay has two braces extending from the bottom of the columns to the outside of the link. The brace bays have links that are 0.61m long for the first four floors, with a link half the length, 0.3m, at the roof. Gravity loading is considered in the design and is acquired from a typical office loading for floors below the roof and snow loading at roof, where the tributary width is taken as a half bay length. The gravity load at the roof, and floors are given as $w_{\text{roof}} = 12.6 \text{ kN/m}$ and $w_i = 22.9 \text{ kN/m}$, respectively.

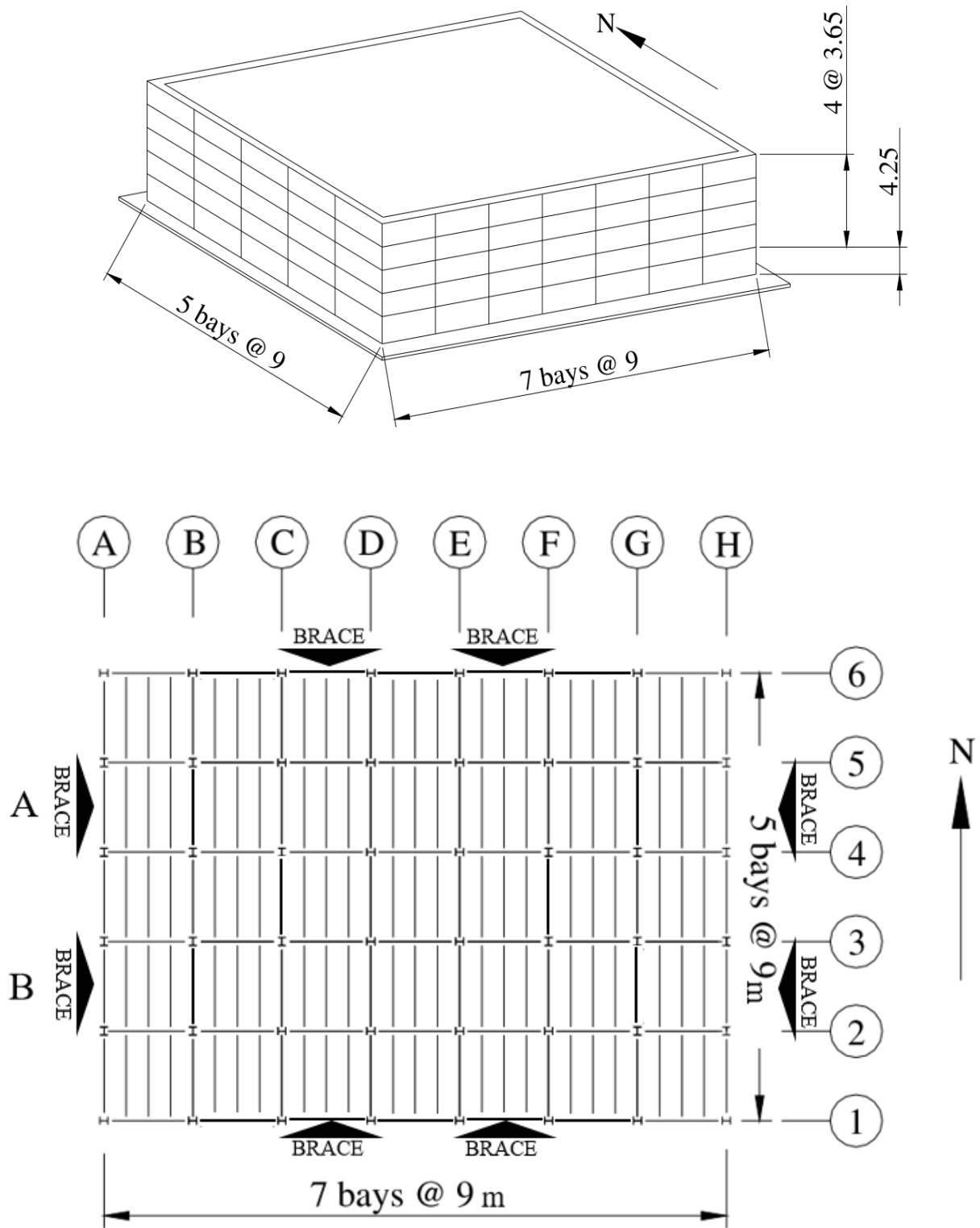


Figure 13. Typical prototype structure [37] (top) Isometric layout (bottom) Plan layout.

This study assumes that the REBF links are decoupled from the gravity system and will only be designed to resist seismic loads. It is also assumed that the floor acts as a rigid diaphragm, and thus causes the link to experience negligible axial load, and is therefore the link is exempt from axial design. The intention of the research is also to develop a design procedure that safely employs the use of replaceable, bolted links, which typically gives links that are of smaller size than the beam members between the brace and the column.

2.3 ESFP – Specific Application

In reference to section 1.1.1, ESFP is employed to design the SFRS, two sets of REBFs running parallel to each side of the building. The next section discusses the parameters used to establish a design base shear and how that value is used to size the links of the frame.

2.3.1 ESFP Parameters

As noted from the base shear formula in section 1.1.1, there are five different parameters that are required to establish the expected base shear the building will experience. The parameters from section 1.1.1 are quantified as follows

- $S(T_a)$: The spectral acceleration based on the fundamental period of the structure. Clause 4.1.8.11 3) b) of NBCC 2015 [2] gives a formula: $T_a = 0.025h_n$ which is used to predict the fundamental period of braced frame structures. This equation presents the building having a period of 0.47s. This value is used in conjunction with the foundation factors reported in clause 4.1.8.4 to determine the acceleration based on the Vancouver UHS. However, a period of 0.71 was used for design, which is what the modal analysis

determined from the initially sized structure. Re-iterating and accounting for site conditions the anticipated building acceleration is given as, $S(0.71) = 0.612g$

- W : The seismic weight of the building, which is any mass in the structure that is activated and transformed into a force at the time of acceleration, is taken as the numbers reported earlier in section 3.1, $W = 54687kN$
- I_e : is the importance factor attributed to the building use and is quantified as 1.0 corresponding to normal building use in NBCC 2015
- M_v : is the higher mode effect factor also reported by NBCC 2015 in Table 4.1.8.11 and is quantified as 1.0 for this structure as $S(0.2)/S(5.0) = 10$
- R_d is the ductility factor associated the type of SFRS chosen and in this case, has a value of 4.0 per Table 4.1.8.9 of NBCC 2015
- R_o : is the overstrength of the system (including material and inherent mechanisms in the design) and is given a value of 1.5 from Table 4.1.8.9 of NBCC 2015

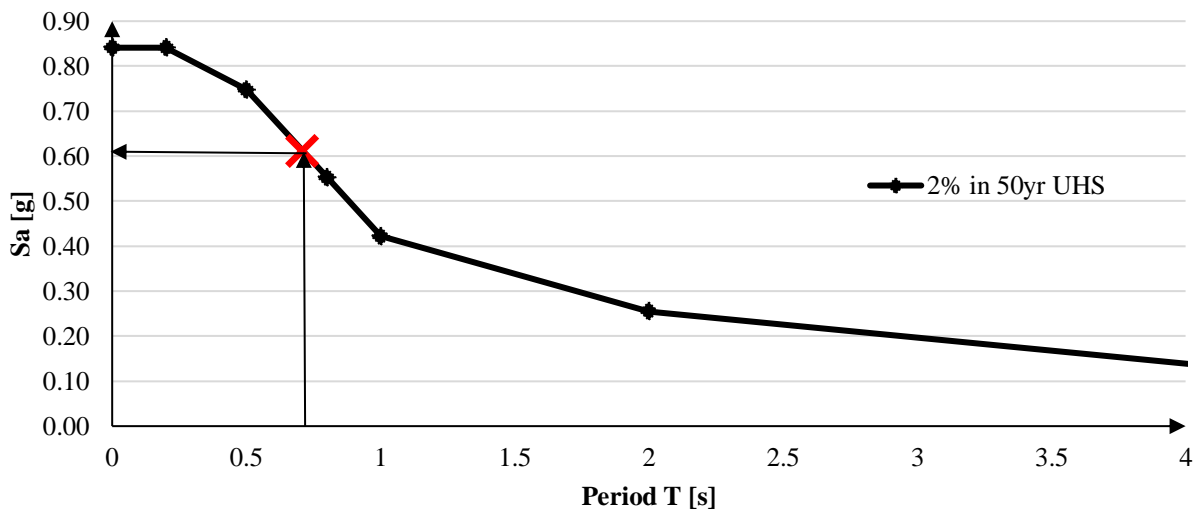


Figure 14. Vancouver Uniform Hazard spectrum with period of interest marked with “X”

As noted, these parameters establish the maximum base shear the structure is expected to experience, while accounting for a base shear reduction due to system overstrength and ductility. However, clause 4.1.8.11 2) a) - c) NBCC 2015 gives further limits and bounds to the applied base shear to ensure the building is not under designed for higher period structures and not overdesigned to account for period elongation of stiffer, shorter period structures.

$$V_e = \frac{S(2.0)M_v I_E W}{R_d R_o} = 3846 \text{kN}; \text{ Lower Limit} \quad (21)$$

$$V_e = \frac{2S(0.2)I_E W}{3R_d R_o} = 5110 \text{kN}; \text{ Upper Limit 1} \quad (22)$$

$$V_e = \frac{S(0.5)I_E W}{R_d R_o} = 6818 \text{kN}; \text{ Upper Limit 2} \quad (23)$$

In this case, the base shear lands within the bounds given by the code.

$$V_e = \frac{S(T_a)M_v I_E W}{R_d R_o} = 5574 \text{kN} = > 2787 \text{kN} / \text{ Dual frame} \quad (24)$$

A common practice in industry is to increase the base shear by 10% to account for accidental torsion, inherent with construction irregularities.

$$V_{\text{Design}} = 1.1 * V_e = 3065 \text{kN}; \quad 11.2\% \text{ of seismic weight, } W$$

Furthermore, to account for the “whipping” effect that is experienced at the top storey of buildings, NBCC 2015 gives a condition in clause 4.1.8.11 7), that attributes a portion of the base shear to be applied at the top storey. As the building has a period of 0.71s, 305kN was taken from the design base shear and applied as a point load at the top.

The basis for attributing the spectral acceleration to the building is purely estimation, as noted by the building period equation based on height and SFRS category. A dynamic modal analysis can be used to validate the use of a higher period per clause 4.1.8.11 3) d) ii) NBCC 2015

but is to be less than twice the period calculated using the formula earlier. This period can be used to estimate the spectral acceleration, and decrease the potential base shear, however the code limits the increase to twice that which was originally calculated. This flexibility is convenient from a designer point of view, however, to develop a model for modal analysis a complete model must first be sized from the initial calculated base shear. This is the inherent frustration encountered by the designer – where the model often does not match the calculated period. Another frustration is encountered when the model is sized to resist the calculated base shear, but is found to not meet the drift limitations set out by the code. Such frustrations inevitably warrant a re-design and sizing of the system; thus, iteration must take place until all variables are coherent. Member sizing and model establishment are discussed in the following sections. Table 1 gives the values that were determined based on the site conditions and preliminary analysis.

Table 1. Parameters used for ESFP Design
ESFP Parameters

| | |
|------------------------|-------|
| W (per dual frame, kN) | 27343 |
| Ie | 1.0 |
| Rd | 4.0 |
| Ro | 1.5 |
| T [s] | 0.71 |
| Site Class | C |
| Mv | 1 |
| J | 1 |
| Sa [g] | 0.612 |
| x^*W | 0.112 |
| V [kN] | 3065 |
| Δ_{max} [%] | 2.5 |

2.3.2 Base Shear Distribution

The base shear is vertically distributed to each floor of the structure including the roof. NBCC 2015 provides an equation in clause 4.1.8.11 7) as shown in the following equation:

$$F_x = (V - F_t) \frac{W_x h_x}{\sum_{i=1}^n W_i h_i} \quad (25)$$

Where F_x is, the shear applied at the storey of interest; V is the design base shear; F_t is the whipping force applied at the top of the building; W_x and h_x is the seismic weight and storey height of the level at interest respectively; and the denominator is the sum product of weight and floor height for the building. It is interesting to observe that the storey shear distribution is based directly on the vertical weight distribution of the building. Table 2 presents the force distribution for each storey of the building, where V_i is the link shear demand at the respective level.

Table 2. Force Distribution applied to ESFP model

| Level | F_x [kN] (Single Frame) | V_i [kN] (Single Frame) | V_{link} [kN] (Single Frame) |
|-------|------------------------------|------------------------------|-----------------------------------|
| Roof | 411 | 411 | 166 |
| 5th | 438 | 849 | 344 |
| 4th | 333 | 1182 | 479 |
| 3rd | 228 | 1410 | 572 |
| 2nd | 123 | 1533 | 724 |

2.3.3 Link Sizing

The intent of the model is to employ replaceable links between the braced frame elements, this means the links can be sized independent of the beam sizes. Figure 15 shows how the storey shear is transformed to link shear. The diagram assumes a rigid diaphragm that transfers the storey shear equally between each half bay. The forces are determined based on static equilibrium, which is industry standard as presented by Bruneau [21].

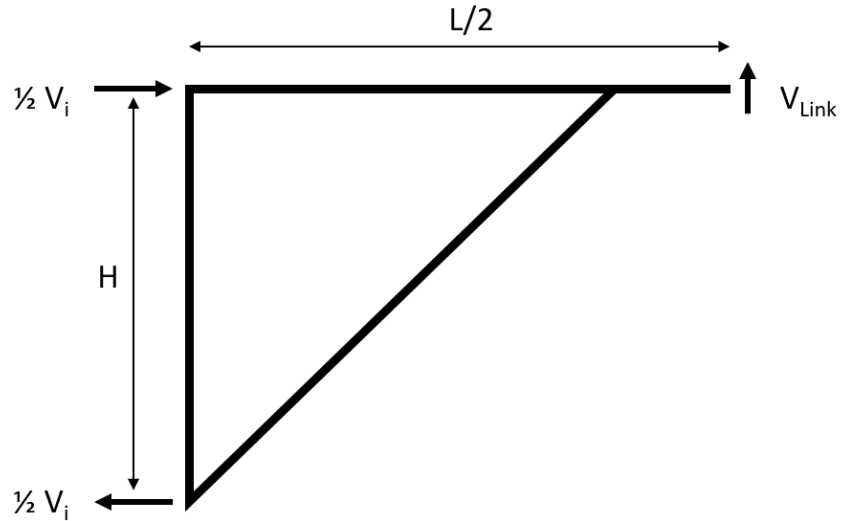


Figure 15. Half bay schematic of static force equilibrium from lateral load on EBF

From the above diagram the force the link is required to resist can be quantified by equation 7 below.

$$V_{Link} = V_i \frac{H}{L} \quad (26)$$

It is interesting to note that this reveals the link strengths being based directly on bay geometry. Table 3 gives the strength design values, the associated link sizes, and their capacities and equation 8 shows the equation from S16-09 used to evaluate the capacity of the section. Where V_y is the design yield strength of the section; V_p is the theoretical plastic strength of the section and V_{pr} is the probable strength of the section, which is determined by increasing the yield strength by an overstrength factor obtained through calibration (see Chapter 4). M_p is the plastic moment calculated from plastic section modulus, Z , and material yield stress F_y . For design purposes, V_p was used to size the links and V_{pr} & M_p were used to capacity design the frame elements.

$$V_p = 0.55AF_y \quad (27)$$

$$V_y = \text{Max}(\varphi_s V_p, \frac{2\varphi_s M_p}{e}) \quad (28)$$

$$V_{pr} = 1.22V_y \quad (29)$$

$$M_p = \varphi_s Z F_y \quad (30)$$

Table 3. Link size and values

| Level | V_{link} [kN] | Section | V_p [kN] | V_{pr} [kN] | M_p [kN-m] |
|-------|------------------------|----------|------------|---------------|--------------|
| Roof | 166 | W150x18 | 168 | 198 | 47 |
| 5th | 344 | W310x28 | 352 | 453 | 140 |
| 4th | 479 | W310x67 | 494 | 635 | 362 |
| 3rd | 572 | W310x107 | 643 | 828 | 611 |
| 2nd | 724 | W310x129 | 790 | 1017 | 745 |

2.3.4 Capacity Design

With the links sized, the next step is to size the members outside of the link. These members consist of the columns, beam and brace elements and are referred to as the frame members henceforth. To ensure only the link yields in the design, the frame members must be designed to remain elastic. This approach is termed as capacity design, and is achieved by applying the probable ultimate strength the link endure, V_{pr} . And the plastic moment capacity M_p at the brace and beam connection. The values used for design are in Table 3. Figure 16 below depicts how the forces are applied to the model, including gravity forces, w_i as discussed at the beginning of chapter 3.

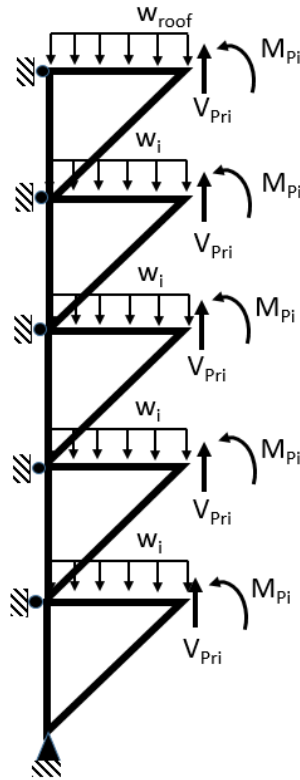


Figure 16. Elastic capacity design model using SAP2000.

The base is pinned to match the design intent and each floor is restrained from lateral movement to simulate the balanced reactions from the frame in motion, as well as to achieve stability to run the analysis. This process yields member sizes that will stay elastic while encountering the probable resistance of the links. Having frame members that remain elastic means localized damage, concentrated on the links, which are designed to be replaceable. The complete frame is presented in the Figure 20.

Table 4. ESFP Non-yielding for each frame

| Level | Column | Beam | Brace | Total Weight [kN] |
|-------|----------|----------|----------|-------------------|
| 5th | W530x72 | W530x72 | W610x91 | 42.03 |
| 4th | W530x72 | W530x72 | W610x101 | 44.23 |
| 3rd | W610x101 | W690x140 | W690x125 | 64.83 |
| 2nd | W690x140 | W690x140 | W690x140 | 73.69 |
| 1st | W840x176 | W690x140 | W840x176 | 93.69 |

Total Frame Weight = 318 kN

2.4 EEDP – Specific Application

This section applies the steps outlined in section 2.1 to develop a model using EEDP. The general steps are applied to the prototype building in section 2.2 to develop a design for the DREBF. As the building is located in Vancouver, B.C. the NBCC 2015 [2] 2% in 50 year UHS for Vancouver was used to define the MCE shaking intensity. The SLE and DBE levels are taken as $1/6$ and $1/3$ of MCE, respectively. The spectra are shown in Figure 17. The parameters for design are given in Table 5 and figure 18 shows the response of the desired tri-linear system broken into the two primary and secondary systems.

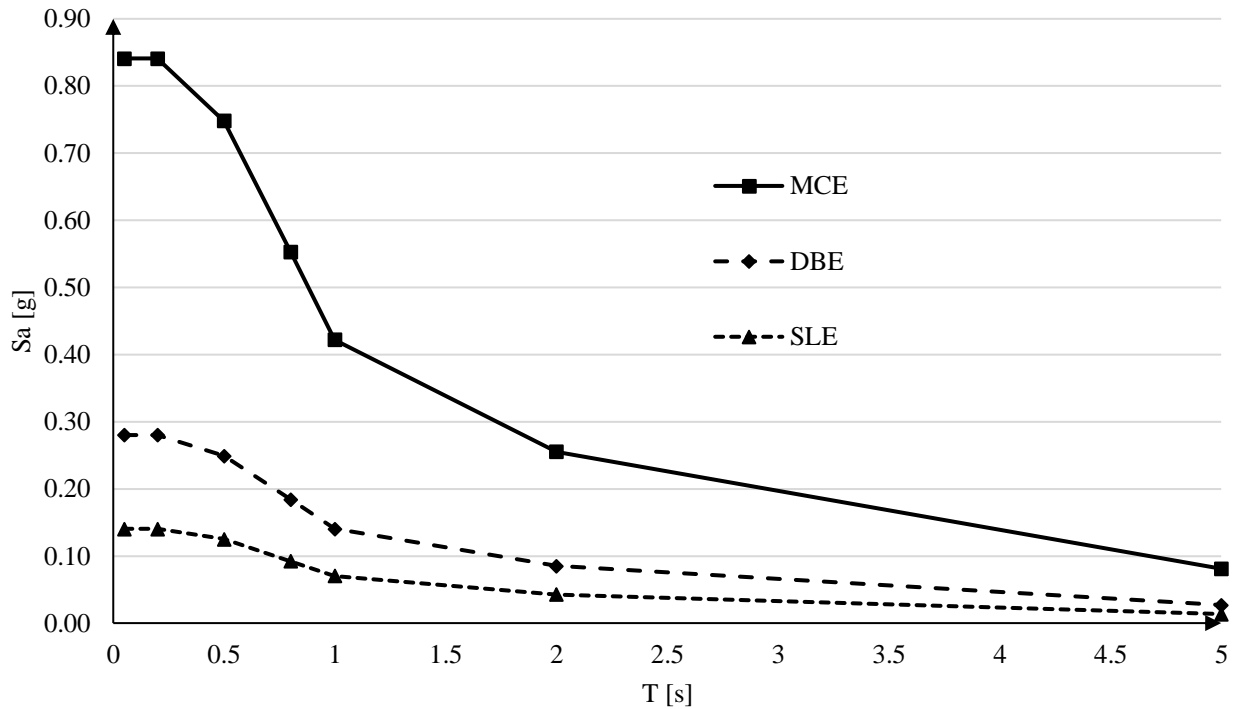


Figure 17. Target spectra for design and ground motion scaling

Table 5. Parameters used for EEDP Design

| EEDP Parameters | |
|------------------------|-------|
| W (per dual frame, kN) | 27343 |
| Co | 1.40 |
| Δy [%] | 0.11 |
| Sa y [g] | 0.090 |
| Fy [kN] | 2448 |
| Δp [%] | 0.17 |
| Sa p [g] | 0.121 |
| Fp [kN] | 3300 |
| T [s] | 0.81 |
| γa | 2.42 |
| γb | 4.40 |
| Δu [%] | 0.46 |

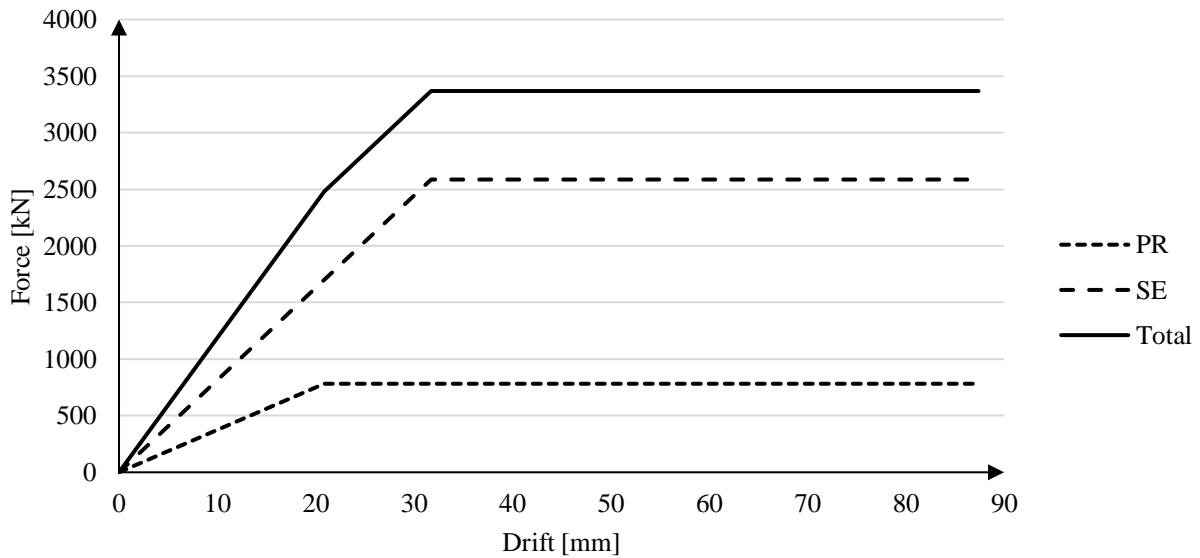


Figure 18. Primary, Secondary and Total building design static response

2.4.1 Plastic Design of Yielding Members (Shear Links)

The links in the DREBF are elements of the structure intended to yield under specific loading, as noted in the past sections. For construction convenience, the design of these links has two important objectives:

1. Be constructed with commonly available W-shapes (avoid using proprietary products)
2. Be easily replaced (replaceable links have been used in the past and S16-09 and AISC [27], [38], [39] give information on how the links need to be detailed to be replaceable and stable)

With these objectives considered, the designer has a selection of link sizes limited to that which is commonly available during construction. From the sizes available, as is intuitive, the designer selects the size that matches or exceeds the demand calculated for the link. The demand on the link is calculated using the principles of work and kinematic theory.

The following outlines the process that uses the kinematic theory with specific free-body diagram reference to Figure 12. Where, Δ_i is the global drift of each storey of the building; θ_p is the rotation of the building columns to cause plastic hinging of the links; H_i is the storey height of each floor with respect to the base; L is the bay width; and δ is the link deformation. It is interesting to note that assuming rigid frame motion, the link deformation is constant up the building, as it is dependent only on the bay width and a single plastic rotation.

$$W_{ext} = \sum F_{pri} \Delta_i; \quad \Delta_i = \theta_p H_i \quad (31)$$

$$W_{int} = \sum V_{link,i} \delta; \quad \delta = L \theta_p \quad \therefore = \sum \beta_i V_{link,roof} L \theta_p \quad (32)$$

$$W_{ext} = W_{int} \quad \therefore V_{link,roof} = \frac{\sum F_{pri} H_i}{\sum \beta_i L} \quad (33)$$

$$V_i = V_{link,roof}\beta \quad (34)$$

Having the design force for each link determined, V_i , it is possible to size them. Similar to the static design, EEDP employs conventional W-shape members to act as fuses. To exploit the plastic capabilities and approximate the hysteretic energy behaviour of the link, the probable shear strength is used to size the links to the demand. The equation below shows how the probable strength capacity of each link is calculated. The probable strength is also used for the capacity design of frame elements. Different from the static procedure, M_p is taken as $V_p * e/2$, which is applied at the end of the brace-beam connection as shown in Figure 19.

$$V_{design} = V_{pr} = 1.22 * 0.55AF_y \quad (35)$$

Table 6. EEDP Link Primary (top) and Secondary (bottom) sizes and values

| Level | Vpri [kN] | Section | Vpr. [kN] | Mp. [kN-m] |
|-------|-----------|---------|-----------|------------|
| Roof | 105 | W100x19 | 174 | 53 |
| 5th | 202 | W150x18 | 205 | 63 |
| 4th | 267 | W200x22 | 296 | 90 |
| 3rd | 309 | W200x31 | 311 | 95 |
| 2nd | 331 | W200x42 | 342 | 104 |

| Level | Vsei [kN] | Section | Vpr. [kN] | Mp. [kN-m] |
|-------|-----------|----------|-----------|------------|
| Roof | 347 | W200x42 | 342 | 104 |
| 5th | 668 | W310x74 | 675 | 206 |
| 4th | 884 | W310x129 | 964 | 294 |
| 3rd | 1023 | W310x143 | 1047 | 319 |
| 2nd | 1096 | W310x158 | 1173 | 358 |

2.4.2 Capacity Design

The capacity design of the non-yielding elements is carried out by applying the probable link forces and associated induced moments on a half bay column tree model as shown in Figure 19. Following PBPD, a restoring force is applied to each floor, replacing the supports applied in the static approach. The restoring forces are calculated based on the applied probable forces and gravity loads that induce a moment around the base. Because the base is intended to be designed as a pin connection, the restoring forces are verified by showing that the base moment is equal to zero. Note that the model must be built with a fixed base to ensure mathematical stability, despite the design having a pin based connection. Based on the direction of loading, the restoring force is calculated differently. The equations to calculate the right and left loading directions, $F_{i,right}$ and $F_{i,left}$, are given respectively in the following equations, note the difference is whether gravity induces a moment in the same or opposite direction as the probable link forces. Where L_b is the length of the beam, w_i is the gravity load on the frame, h_i is the storey height with respect to the base and C_{vi} is factor calculated earlier in equation 19.

$$F_{right} = \frac{\sum_i^n (M_{pi} + L_b V_{pri} - \frac{L_b w_i^2}{2})}{\sum_i^n C_{vi} h_i} \quad (36)$$

$$F_{left} = \frac{\sum_i^n (M_{pi} + L_b V_{pri} + \frac{L_b w_i^2}{2})}{\sum_i^n C_{vi} h_i} \quad (37)$$

$$F_{i,right} = C_{vi} F_{right} \quad (38)$$

$$F_{i,left} = C_{vi} F_{left} \quad (39)$$

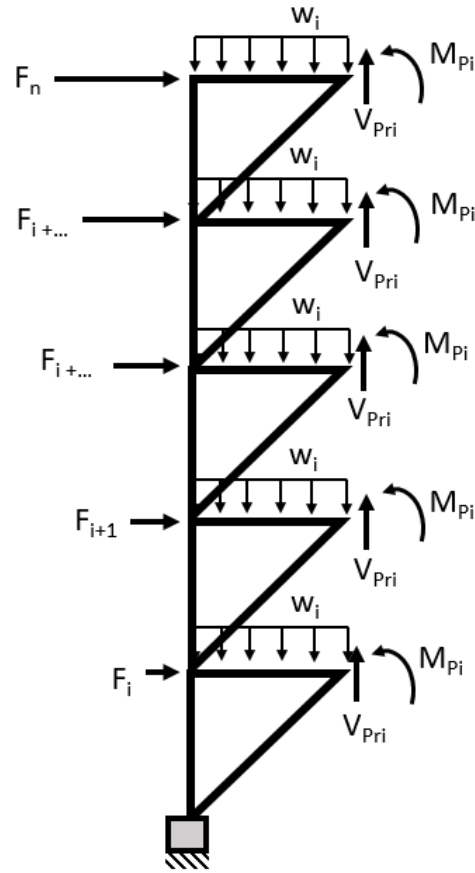


Figure 19. EEDP half-bay column tree elastic capacity design model using restoring forces

Table 7. EEDP Non-yielding elements Primary (top) and Secondary (bottom) sizes

| Level | Column | Beam | Brace | Total Weight [kN] |
|-------|----------|---------|----------|-------------------|
| 5th | W460x60 | W410x46 | W530x66 | 15.29 |
| 4th | W610x82 | W460x52 | W530x74 | 18.24 |
| 3rd | W610x101 | W460x60 | W610x92 | 22.22 |
| 2nd | W610x101 | W530x66 | W610x92 | 22.72 |
| 1st | W690x125 | W460x60 | W610x101 | 27.21 |

| Level | Column | Beam | Brace | Total Weight [kN] |
|-------|----------|----------|----------|-------------------|
| 5th | W410x39 | W530x66 | W610x92 | 18.27 |
| 4th | W460x60 | W610x101 | W610x113 | 24.96 |
| 3rd | W690x125 | W610x101 | W760x147 | 33.32 |
| 2nd | W760x161 | W690x125 | W760x161 | 39.41 |
| 1st | W840x210 | W690x125 | W760x173 | 48.09 |

Total Frame Weight = 270 kN

Chapter 3: Numerical Modelling

The focus of this chapter is to use the analytical models from the previous chapter, each from their respective design procedures: ESFP and EEDP. Each model represents the SFRS for the building described in chapter 2. Section 4.1 highlights how the numerical model is developed and the program used to undergo analysis. Calibration is explained in section 4.2 discusses the process of taking real data and linking it to a numerical approximation. Section 4.3 discusses the period of each model as compared the initial design assumption.

3.1 Numerical Model Description

OpenSees is used as the platform for numerical modelling and analysis. OpenSees is a powerful research tool that enables the user to undergo transparent non-linear analysis while recording specific response information. Specific elements can be defined through various techniques to model different members of a structure. With the intention of isolating the non-linear properties and behaviour of the shear link connection of the DREBF, the links are modelled with a force-based fibre element that simultaneously employs a shear aggregator. The other frame elements are not expected to undergo plastic deformation, and have been modelled using elastic elements. The link connecting the two frames also uses an elastic truss element with a large elastic modulus to simulate a rigid diaphragm connection. Elastic truss members were also used for the brace members to simulate a bolted connection between the frame and braces; a bolted connection between the beam and column is also simulated using a zero-length element between the column and beam that has effectively zero stiffness in rotation. These simulations seemed appropriate and necessary considering conventional construction practices. The model employs equal degree-of-

Gravity loads are considered on the model equal to those discussed in section 2.2. They are modeled as uniformly distributed along the beam elements – note that the links are exempt from this as they are assumed to be de-coupled from the gravity system. The gravity loads are applied during ground motion analysis and a geometric transformation is used that accounts for P-Delta contributions. Mass is added to the system for period and base shear calculations and is defined at the top of each column element in the direction of shaking. The mass is equal to the sum of each floor seismic weight (see section 2.2) divided by gravity and split between two systems and four nodes per floor. A schematic of the EEDP DREBF model built in OpenSees is shown in Figure 21.

3.2 Calibration

To validate the use of a numerical analysis which approximates realistic non-linear behaviour, a calibration procedure is undertaken. Dusicka and Lewis [24] reported the results of seismic testing of replaceable W-shape links in a full scale model. OpenSees is used to develop an identical full scale model which performs the same testing protocol. The shear links are nonlinear elements modelled using fibre elements combined with a shear aggregator and use Steel02, “Giuffrè-Menegotto-Pinto” material with a yield stress, F_y of 345MPa for steel. This process creates a member that can capture simultaneous non-linear behaviour in bending and shear (though it captures the simultaneous responses, it does not capture the response due to interaction between them), without accounting for the length of the member in the material definition. Although this process creates a more “cumbersome” and complex element when compared to using a zero-length hinge, the author felt it worth the effort to keep the tangible connection between a numerical

element and the realistic properties the element is approximating. This effort is realized in the material definition.

3.2.1 Experimental Results

Three different lengths of links were tested, short, intermediate and long, as defined by the state in which they yield. Short links yield in shear and are defined by the expression: $eV_p/M_p < 1.6$. Intermediate links are considered to yield in bending and shear and are defined by $1.6 < eV_p/M_p < 2.6$. Long links yield in bending and are defined by $eV_p/M_p > 2.6$. Only the short link test was used for calibrating the model, as conventional design employs shear links (short links). Dusicka and Lewis prepared test results from a short link experiment that was detailed using standard construction detailing convention [27]. The specific experiment of interest consisted of two 3600mm tall W360x216 (W14x145) columns connected at their mid-point by the member being tested, which in this case was a W310x143 (W12x96) 1320mm (52") in length. The base of the columns is pin-restrained and an actuator is attached to the top of each column with pin connection. A reverse cyclic deformation protocol of EBF links (AISC 2005) was performed on the link by the actuator.

3.2.2 Numerical Calibration Model Description

Following suit with the test set up discussed in the previous section, a numerical model was approximated using OpenSees. The base restraints, lengths, sizes and load protocol are identical to those used in the actual test setup. The columns were approximated with elastic elements (assuming no yielding on the test experiment) that mimic the gross properties of their respective sections. The link was modelled using the same fibre and shear aggregator combination as discussed in section 3.2. Material Steel02 was used to define the bending behaviour of the fibre

element. Because bending is assumed to not govern the yielding behaviour of the link, the default material characteristics are used that define 350MPa steel are used and not calibrated. However, the shear aggregator will govern the yielding behaviour, therefore the material defining this response is to be calibrated. Steel02 is again used as the material for yield behaviour definition in the shear aggregator.

3.2.3 Calibration Results

As mentioned, the numerical model was setup to mimic the full scale experimental model, including applying the cyclic load at the top of each column and allowing for elastic deformation of the columns to be a part of the link response. The link response was captured by measuring the displacement at the top of the column and shear force response at the end of the link. The rotation (θ_p) of the link is simply equal to the displacement at the top of the column (Δ) divided by the height (H) of the column, assuming the elastic deformations in the column are negligible. To achieve a numerical response that matched the experimental, parameters were given as such for the shear aggregator material Steel02: $F_y = 1047\text{kN}$ ($1.22 \cdot 0.55 A_w F_y$), $E = 348\text{MN}$ (GA_w). the response is given in Figure 22.

$$\theta_p = \Delta/H \quad (40)$$

Table 9. OpenSEES Steel02 material definition (values shown in kip & in)

| Fibre Bending Material | | | | | | | | | | | | |
|----------------------------------|--------|------|-------|-------|------|-------|------|-------|----|-------|-----|--------|
| Material | matTag | Fy | E | b | R0 | cR1 | cR2 | <a1 | a2 | a3 | a4> | <sig0> |
| Steel02 | 2 | 50.8 | 29000 | 0.05 | 18.5 | 0.925 | 0.15 | 0 | 1 | 0 | 1 | 0 |
| Shear Aggregator Material | | | | | | | | | | | | |
| Material | matTag | Fy | E | b | R0 | cR1 | cR2 | <a1 | a2 | a3 | a4> | <sig0> |
| Steel02 | 884 | 237 | 78256 | 0.003 | 18.5 | 0.925 | 0.15 | 0.033 | 1 | 0.033 | 1 | 0 |

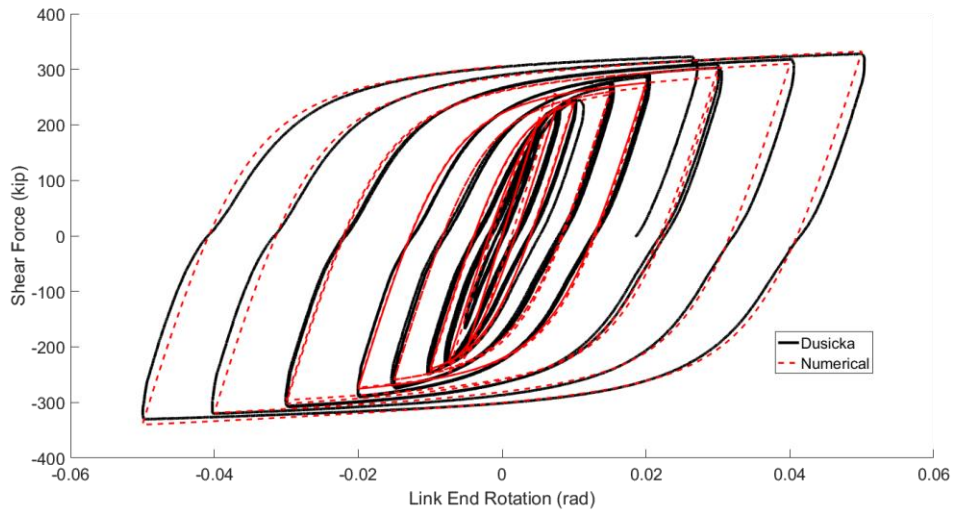


Figure 22. Calibration Experimental test and numerical overlay

The results reveal that the direct use of standard W-shape properties as conventionally calculated, is reasonable in estimating the member response. A factor of 1.22 is necessary to be applied to the shear yield strength of the section; the use of the shear modulus, G , multiplied by the web area, A_w is a good representation of the shear stiffness of the element and is the direct input for the shear aggregator material. It was this realization that the author felt was important to reflect in the design as noted earlier. Post yielding stiffness was taken as 0.3% of the shear modulus to account for strain hardening of the steel. It must also be noted that cyclic hardening was observed in the calibration tests and parameters ‘ a_1 ’ and ‘ a_3 ’ were adjusted to account for that in the hysteretic behaviour. These properties were then used to define each plastic capacity response of the chosen link sizes. It is vital to carry this process out to ensure the hysteretic response is reasonable, as the NLTHA is dependent on such responses.

3.3 Comparison of Design and Model Time Period

Table 10 shows the values of the time periods which was estimated during the design phase and the fundamental time period calculated in OpenSees. The real state of the building for both ESFP and EEDP is simulated by employing an elastic frame and calibrated W-shape links. In design, EEDP assumes rigid frame elements and therefore neglects elastic frame deformation and results in individual link stiffness that is much lower than can be achieved using the standard W-shapes in practice. The combination of a softer than rigid frame and stiffer link elements produced a good trade-off in the period calculation.

Table 10. Comparison of design and model fundamental period

| Design | Period from Design | Period from Model | Error |
|---------------|---------------------------|--------------------------|--------------|
| EEDP | 0.81s | 0.75s | 7.4% |
| ESFP | 0.47s | 0.71s | 51% |

Chapter 4: Evaluation of Seismic Performance

This chapter presents the results of both the Nonlinear Static Analysis (Pushover) and Nonlinear Time History Analysis (NLTHA) of the finite element models developed in the previous Chapters. The NLTHA uses a suite of ground motions of varying intensities corresponding to the seismic hazard of the building location. Section 5.1 presents the ground motions used for NLTHA and how the ground motions were scaled and selected. The results of the Pushover analysis are given in section 5.2. Section 5.3 presents and discusses the results from the NLTHA on each model. The results are further interpreted in section 5.4 where Performance Based Earthquake Engineering (PBEE) evaluation of the retrieved data is presented.

4.1 Ground Motions

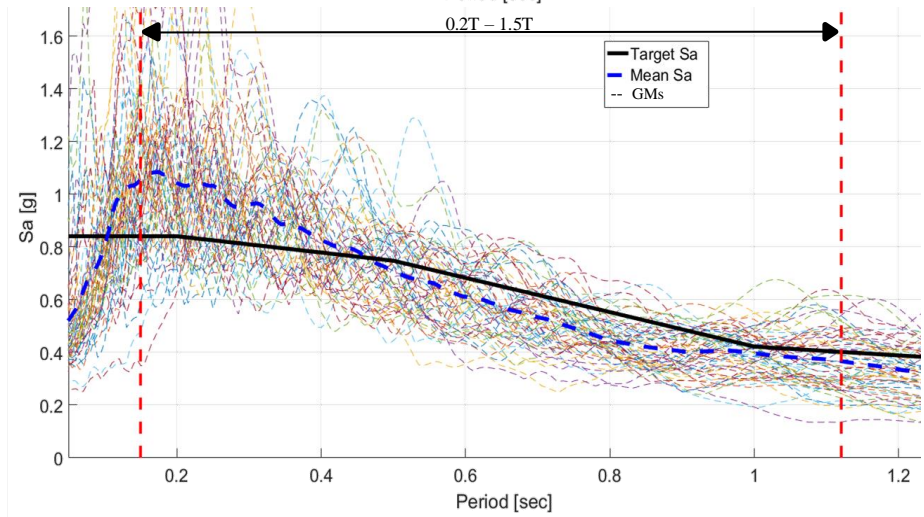
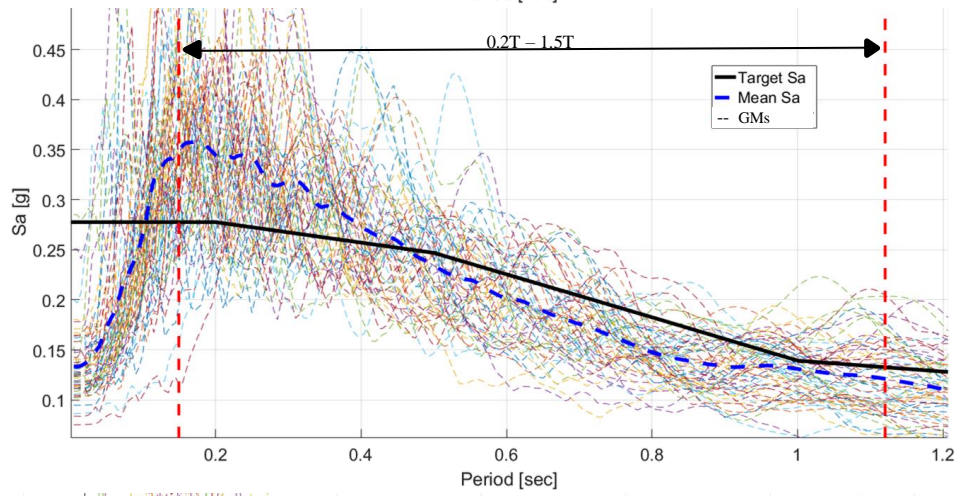
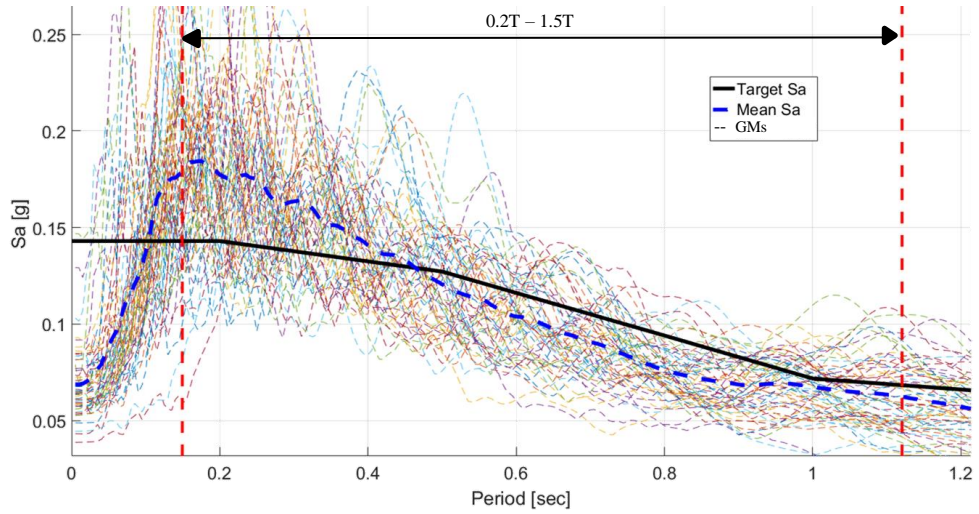
The two buildings are assumed to be in Vancouver B.C. The Pacific southwest region of Canada introduces a unique seismic geography in that there is probability of encountering three different types of ground motions. Crustal and subcrustal ground motions are common and develop the lower end of the seismic risk spectrum for the region. The infamous Cascadia subduction zone which extends up the west coast, ends approximately 50km west of Vancouver Island. Subduction ground motions make up the higher end of seismic risk for Vancouver. With this considered, the author intended to find ground motion records from all three different types of events. The ground motions were selected from Pacific Earthquake Engineering Research (PEER) centre Next Generation Attenuation (NGA) database [40] based on a Probable Seismic Hazard Analysis (PSHA) as reflected in Michael Murphy's [37] ground motion selection. The PSHA revealed the site to be vulnerable to earthquakes within 80km and having max magnitude of 7.7Mw, however

the range was broadened to acquire more records. As appeared reasonable, this paper adopted the ground motions used in Murphy's analysis and added 8 subduction ground motion records, 2 records from 4 different earthquake events. The University of British Columbia's second generation ground motion database was used to acquire the extra subduction records. These ground motions are then amplitude scaled between 0.2 T and 1.5 T to match the target acceleration spectra shown in Figure 17, where T is the fundamental vibration period of the prototype buildings. Figure 23 shows the matched scaled response spectra to the target spectrum. The scaling factors were calculated using a theory that minimizes the Mean Squared Error (MSE) between the ground motion response spectrum and Vancouver UHS. As noted in section 3.3.1, EEDP sets the performance objectives for design as the NBCC 2015 2% in 50 year UHS for Vancouver for MCE shaking and the SLE and DBE levels are taken as $1/6$ and $1/3$ of MCE respectively.

Although, it is not necessary to test the ESFP model to all the shaking intensities, the same process was carried out for each model to develop a grasp for the different performance of each design. Of the 60 ground motions that were scaled, only the motions that yielded a MCE scale factor between 0.5 – 5 were considered suitable for analysis, to try to preserve the spectral shape of each record, while matching the intensity to that expected in Vancouver. A total of 29 records were used for non-linear analysis purposes. Table 11 shows the list of the records with the corresponding scale factors at different hazard levels. Each record provided 2 sets of ground motions representing shaking in orthogonal directions, with exception to the Northridge and Iripinia ground motions that each provided three records and "Loma Prieta" which provided only one record.

Table 11. List of ground motions used for analysis with EEDP model

| Earthquake Name | Year | Magnitude | Mechanism | Scale Factors | | |
|----------------------|------|-----------|-----------------|---------------|------|------|
| | | | | MCE | DBE | SLE |
| "Hokkaido Japan" | 1993 | 7.7 | Subduction | 1.95 | 0.64 | 0.33 |
| "Constitucion Chile" | 2010 | 8.8 | Subduction | 0.49 | 0.16 | 0.08 |
| "Michoacan Mexico" | 1985 | 8.1 | Subduction | 2.81 | 0.93 | 0.48 |
| "Tohoku Japan" | 2011 | 9.0 | Subduction | 0.64 | 0.21 | 0.11 |
| "Chi-Chi_ Taiwan" | 1999 | 7.6 | Reverse Oblique | 1.48 | 0.49 | 0.25 |
| "Kocaeli_ Turkey" | 1999 | 7.5 | strike slip | 3.1 | 1.02 | 0.53 |
| "Northridge-01" | 1994 | 6.7 | Reverse | 3.35 | 1.1 | 0.57 |
| "Loma Prieta" | 1989 | 6.9 | Reverse Oblique | 2.05 | 0.68 | 0.35 |
| "Coalinga-01" | 1983 | 6.4 | Reverse | 3.31 | 1.09 | 0.56 |
| "Irpinia_ Italy-02" | 1980 | 6.2 | Normal | 3.1 | 1.02 | 0.53 |
| "Victoria_ Mexico" | 1980 | 6.3 | strike slip | 0.84 | 0.28 | 0.14 |
| "Imperial Valley-06" | 1979 | 6.5 | strike slip | 2.01 | 0.66 | 0.34 |
| "Tabas_ Iran" | 1978 | 7.35 | Reverse | 1.34 | 0.44 | 0.23 |
| "Gazli_ USSR" | 1976 | 6.8 | Reverse | 0.63 | 0.21 | 0.11 |



(Top) Scaled to SLE

(Middle) Scaled to DBE

(Bottom) Scaled to MCE

Figure 23. Response spectra of scaled ground motions.

4.2 Nonlinear Static Analysis (Pushover)

A pushover of each of these models is shown in Figure 24. The Pushover lateral load distribution up the height of the building is determined from the same pattern as was given in section 2.1. Goel and Chao presented the distribution termed, C_{vi} in this paper, from PBPD to distribute the design base shear up the structure, this is the same ratio used to carry out the Pushover analysis and is given in Table 12.

Table 12. Pushover load distribution up height of structure

| Floor | C_{vi}, Load Distribution |
|--------------|---|
| Roof | 0.32 |
| Level 4 | 0.29 |
| Level 3 | 0.20 |
| Level 2 | 0.13 |
| Level 1 | 0.07 |

The response of the EEDP and ESFP models are compared with the EEDP design curve in Figure 24. The response is congruent with what was designed for in both cases; ESFP yield base shear, $V_y > 3065\text{kN}$ and EEDP second yield, $F_p > 3300\text{kN}$. The chosen performance for the EEDP model was based on the required code based capacity of the ESFP model, which is reflected in the results.

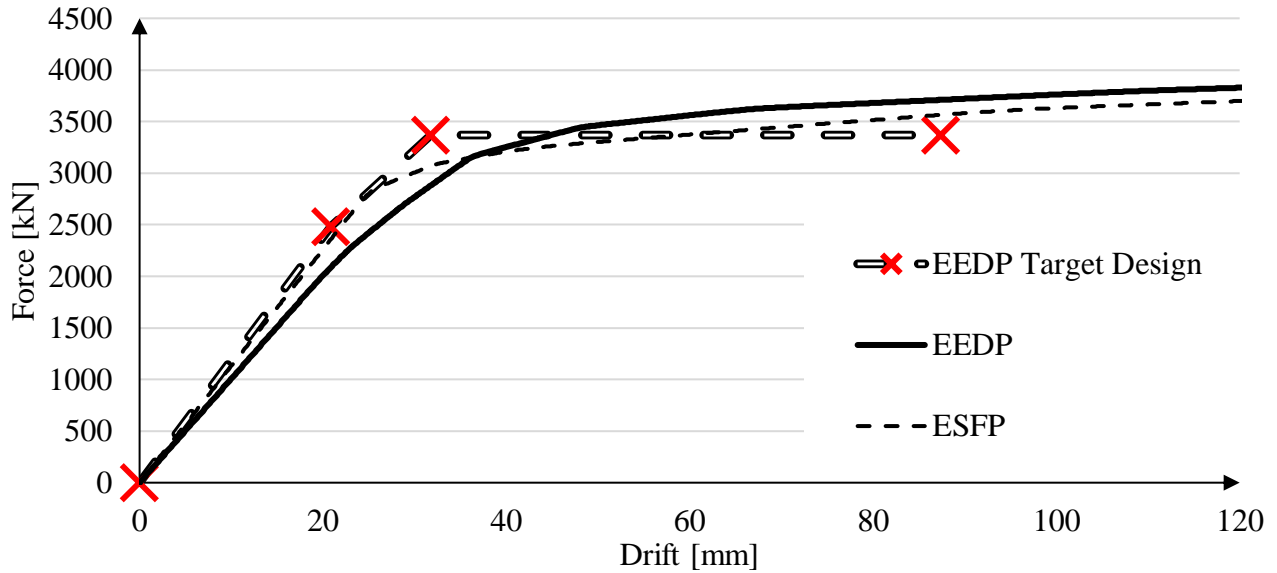


Figure 24. Pushover curves of ESFP and EEDP compared with the EEDP design curve

4.3 Non-Linear Time History Analysis

Nonlinear dynamic analysis is performed using the ground motions listed in Table 11 to examine the seismic response of each EBF system at different earthquake shaking intensities and to compare the results of each design. The full model assigns the seismic masses at the column nodes. Rayleigh damping with 2% damping in the first two modes is used. Figure 25 shows the median roof drift ratios of the two models when subjected to the ground motions given in Table 11. Figure 26 and 27 show the progression of link yielding for the EEDP model as the intensity increases, verifying that the system is behaving as planned. Figures 28 and 29 show the average forces developed in the members outside of the link, verifying that the link was the only element yielding. The EEDP drift values are very close to the targets (Δ_y and Δ_p) shown in Table 5 and Figure 25. At the SLE shaking intensity ($1/6^{\text{th}}$ of the 2% in 50yr. Vancouver UHS) the EEDP design is shown to respond elastically, with the primary links approaching yield. However, it is

interesting to note the links in the ESFP Model have already reached capacity at each storey except the roof at the SLE level.

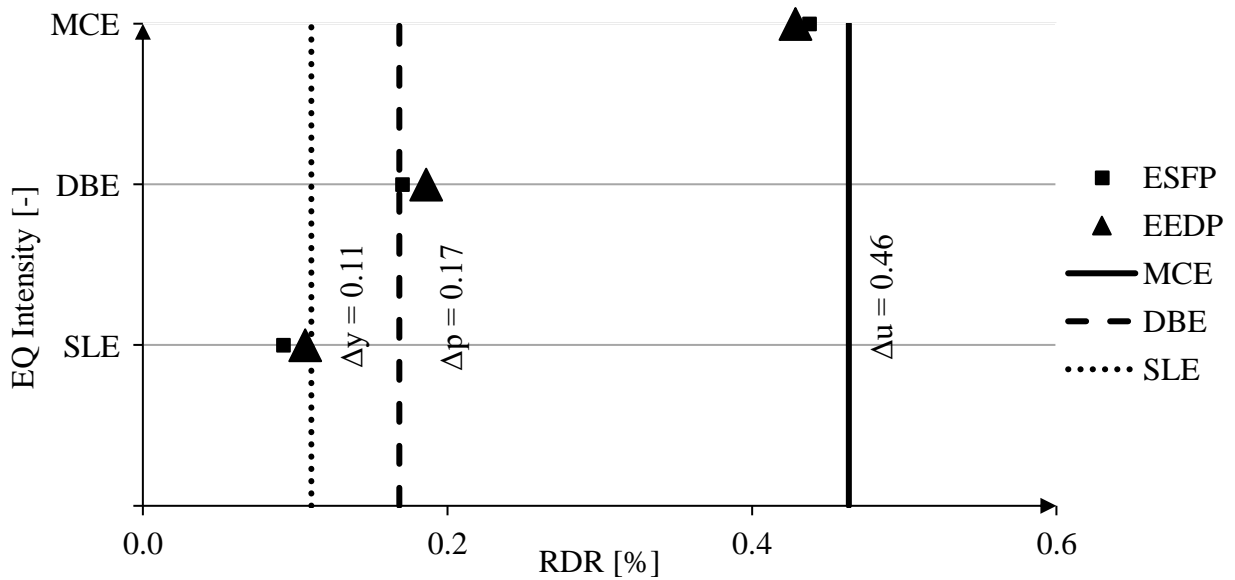


Figure 25. Median Roof Drift Ratio (RDR) comparison.

The results from the NLTHAs show that building performance is possible to be controlled and tuned using EEDP. The models though not the same, employed similar techniques and yielding mechanisms. Figure 25 reveals that the buildings performed similarly in each earthquake. This was to be expected, as the stiffness and mass characteristics did not differ excessively. What is interesting to pull from these results, is that the EEDP model hit the targets that were set out for it at the design stage. EEDP has been shown as an effective design tool that enables the designer to develop a model that will hit specific drift targets based on yielding elements and design spectra.

The yielding elements responded as expected, as shown in figures in 26 and 27. The EEDP model showed that the primary links approached yielding at the SLE level and were fully yielded at the DBE level. Similarly, the secondary links approached yield at the DBE level and were fully

yielded at the MCE level. This shows that control of yield progression and repair implications of this design method are a reality. However, the ESFP model showed links yielding at the SLE level, revealing the lack of yield and damage control.

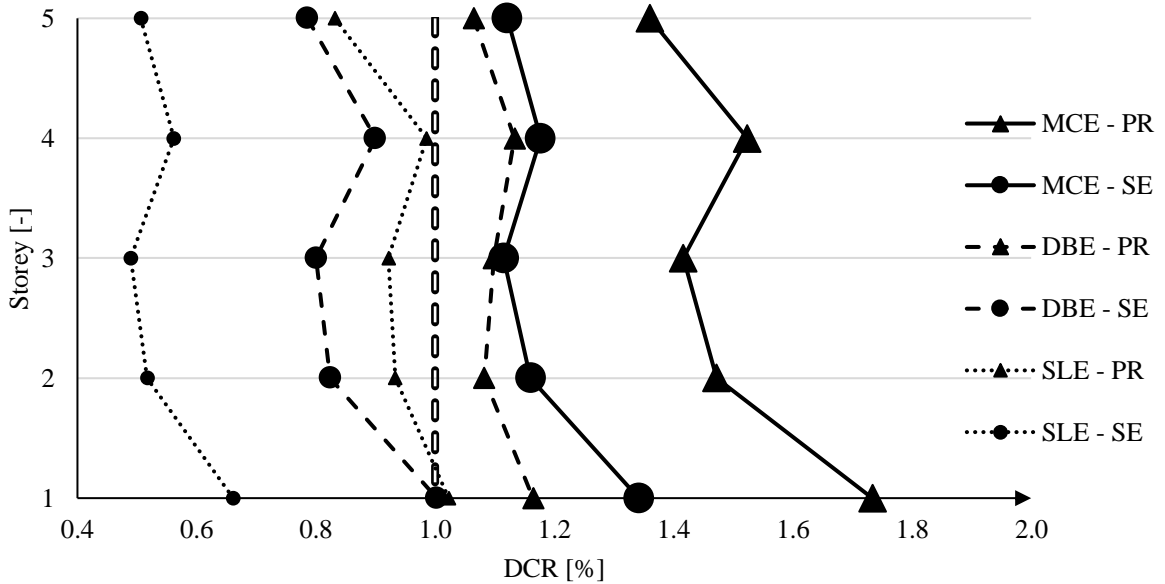


Figure 26. EEDP Link yielding progression.

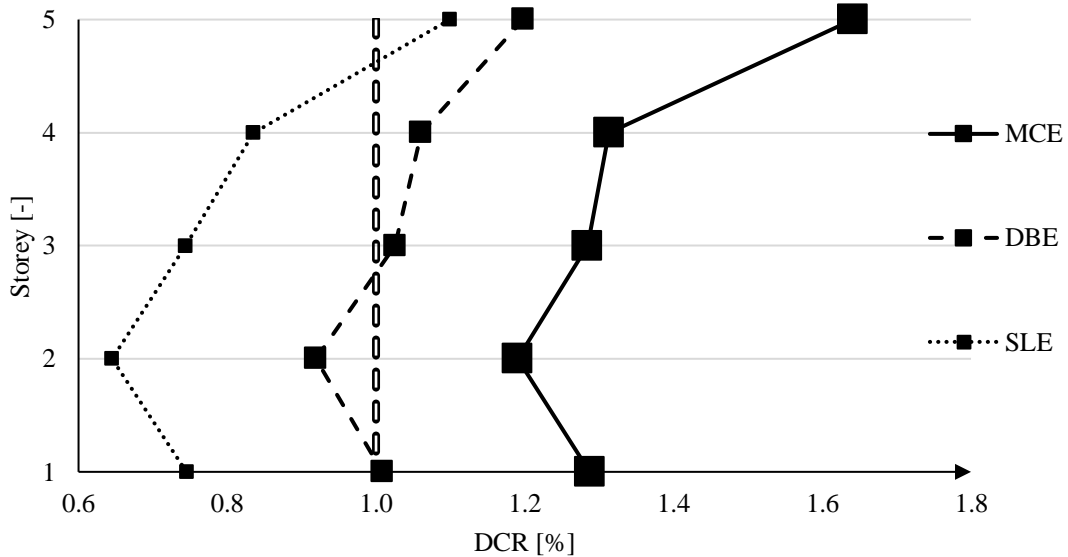


Figure 27. ESFP Link yielding progression.

Table 13. EEDP & ESFP Average Link yielding progression.

| | EEDP | | | ESFP |
|-----|------|------|--|------|
| | PR | SE | | Link |
| MCE | 1.50 | 1.18 | | 1.34 |
| DBE | 1.11 | 0.86 | | 1.04 |
| SLE | 0.94 | 0.55 | | 0.81 |

As noted earlier, EEDP developed a frame model that was noticeably lighter than the ESFP and these results are again reflected when considering the DCR of the frame elements. Figures 28 and 29 show how the lighter frame utilized more of its elastic capacities than the heavier ESFP frame. Both achieved the goal of keeping the gravity frame undamaged, but EEDP managed to do so more economically.

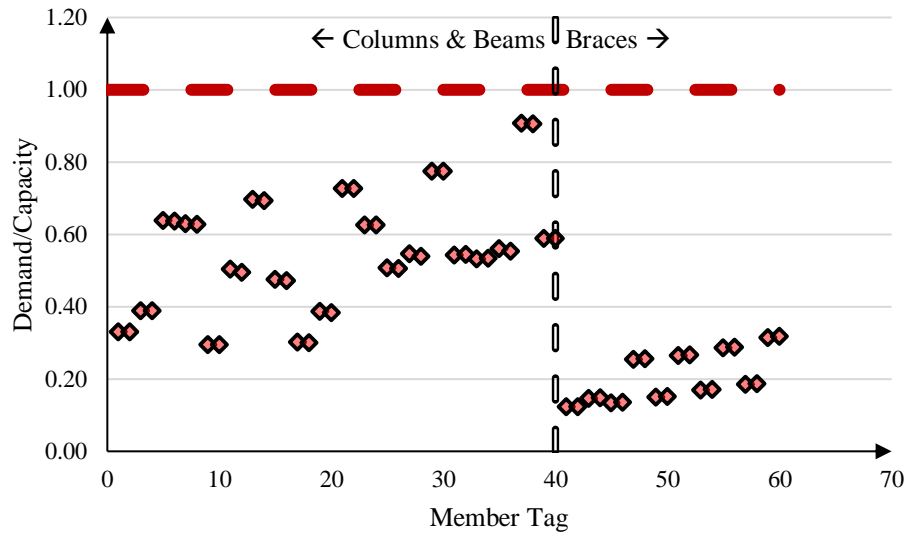


Figure 28. EEDP Frame Element Demand-Capacity Ratio (DCR) at MCE Intensity

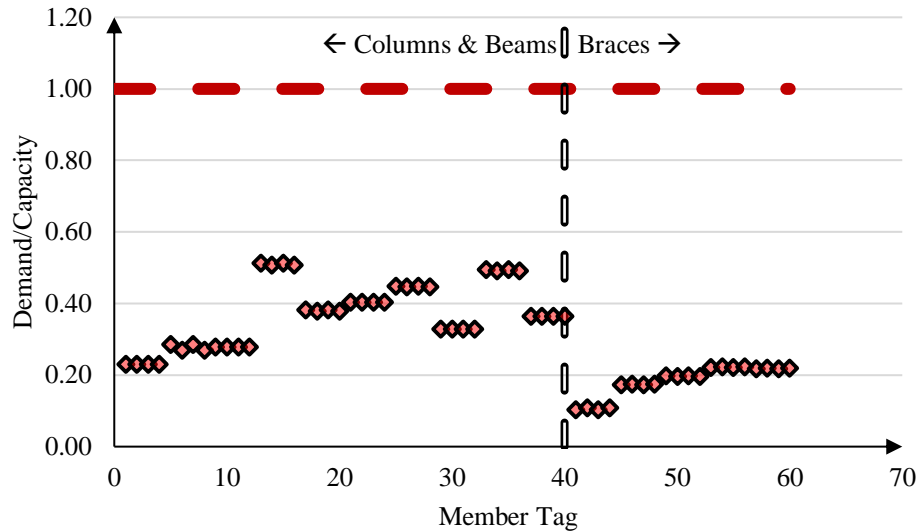


Figure 29. ESFP Frame Element Demand-Capacity Ratio (DCR) at MCE Intensity

As noted earlier, EEDP developed a frame model that was noticeably lighter than the ESFP and these results are again reflected when considering the DCR of the frame elements. Figures 28 and 24 show how the lighter frame utilized more of its elastic capacities than the heavier ESFP frame. Both achieved the goal of keeping the gravity frame undamaged, but EEDP managed to do so more economically.

4.4 Performance Based Engineering Evaluation

From a societal point of view, the essential goal of discovering resilient building models is not only for life safety purpose, but to provide economic sheltering [41]–[44]. Through extensive research and quantification of the typical components that comprise a structure, Yang [44] produces a program that attaches a dollar value to these building components. Building components from the structural lateral system to non-structural cladding to drift sensitive partitions, are all considered in this framework. The program attaches damage states and a dollar

value to each state to represent repair costs. Damage states are indicated, or assumed by specific Engineering Demand Parameters (EDP), which for this case are interstorey drift and floor acceleration. Depending on drift and acceleration values anticipated during the shaking intensities, repair costs for the structure can be calculated by determining the probability of damage on each building component and their corresponding probabilistic repair costs. Because the framework presented by Yang [44] is comprehensive in nature, the default building components and assigned repair dollar values were used in this example of Performance Based Engineering Evaluation (PBEE). This is to say that although a dollar value is attributed to each model, the value itself is not as significant as the comparison. PBEE is carried out on both the ESFP and EEDP models, where each produced usable EDPs used for calculation.

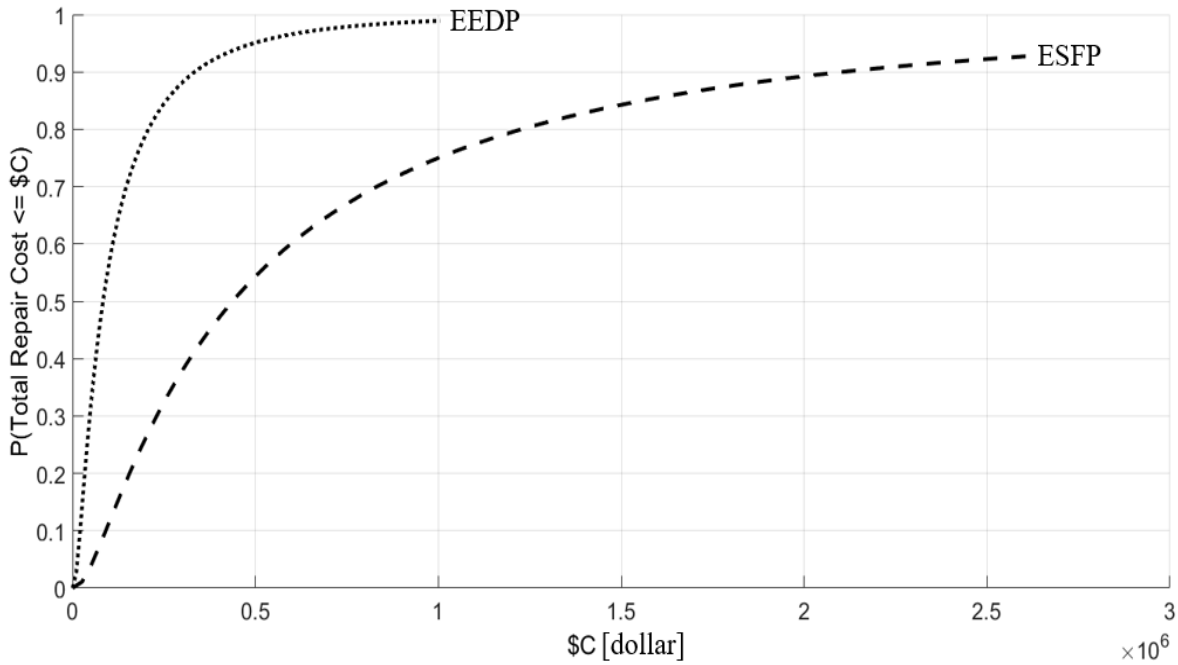


Figure 30. MCE level Repair Cost CDF – (EEDP ‘small dash’, ESFP ‘large dash’)

PBEE shows that based on the drifts and acceleration determined from the NLTHAs that the potential for economic damage using the ESFP design is higher. Figure 30 shows that the probability for the total repair costs of the EEDP curve is effectively under \$1 million, whereas there is only a 75% probability that repair costs for the ESFP design will be under \$1 million. The program also calculated the average annual repair cost to be \$645 and \$292 for the ESFP and EEDP models respectively, which are taken from the assumption that the SLE, DBE and MCE ground shaking events occur with a return period of 72, 475, 2475 years respectively. These monetary results are again evidence of the power of performance based design, which enables the designer to shield selected elements by achieving drift objectives and utilizing localized damaging techniques (fuses).

4.5 NLTHA Conclusion

The results from the different sets of analyses show that both ESFP and EEDP give formidable approaches to design the SFRS for the given building in Vancouver. The EEDP model revealed a more economical and drift controlled model, and introduced a strong way to approximate the actual fundamental period of the building.

Chapter 5: Rehabilitation Design with EEDP

This chapter presents the use of EEDP through the lens of rehabilitation. The DREBF is versatile in application, as a dual frame system can be acquired by adding a single independent frame to operate in conjunction with another independent frame. Rehabilitation is a reality that is being embraced in developing and developed nations, as the seismic hazard for regions becomes made known or increased [45]. Such implications may mean upgrading or seismic rehabilitation of existing structures. Section 6.1 presents the same building as discussed in this paper, however the “existing” state employs only one REBF (which is identical to the secondary frame). The “rehabilitated” state is taken as the tri-linear response presented earlier in this paper. The example model is then compared in section 6.2 between the existing and rehabilitated state through a NLTHA. The goal of this chapter is to present EEDP from another practical design perspective.

5.1 Rehabilitation Example

The same office building is used in this design example, except where two REBFs were employed, only one is used to define the existing state. In this case the secondary frame was used as the only system resisting lateral motion. Because the response of the one frame is lesser than code design, the system was deficient and in need of rehabilitation. EEDP is used to develop a design that will work coincidentally with the existing system and produce the desired tri-linear response. The steps taken to achieve this are given as follows, however the reader is encouraged to reference section 3.2.1, the description of the performance objectives, and Appendix D for calculations:

Define the response of the existing system

The existing system capacity must be known to derive the response of the rehabilitation system that will be implemented.

Define the response of the desired system

The desired response can be given by many variables and is ultimately subject to decisions that have come from collaboration between the owner and designer. In this case, the same performance is required as that of the new design presented in Figure 18 in this paper.

Define characteristics of the rehabilitated system

The period of the existing system will be adjusted due to the new system and is defined using the same functions as described earlier.

Define design spectra

The design spectra are assumed to be derived from the 2% in 50yr UHS for Vancouver, taken as MCE and SLE is defined by the desired yield drift and corresponding base shear which is transformed into a spectral acceleration. As discussed in the main body of this paper, the DBE response relies on the inelastic behaviour of the yielded primary system. To approximate this response, " γ_a " is used to transform the elastic energy to inelastic. The challenge with back calculating this response, specifically for our case in Vancouver, is that, as noted in this paper, specific γ values need to be defined for different building periods and ductilities. The same challenge was encountered when trying to calculate the ultimate drift, as it was unknown which γ_b value to use. However, because this is effectively a back-calculation example that uses the same drift targets and fundamental period as the previous EEDP design, the γ values presented in Table 5 can be used to arrive at the correct results.

The MCE response relies on the behaviour of the SFRS with both the primary and secondary fuses yielded. In this case the UHS for Vancouver is used as mentioned. From this level of shaking and γ_b values the ultimate roof drift, Δ_u can be estimated as shown in equation 23. The design anticipated a fundamental period of 0.99s and 0.81s for the existing and rehabilitated systems respectively, where the OpenSees modal analysis produced a period of 1.06s and 0.75s for each.

5.2 Rehabilitation Comparison

From this example, it is possible to see the power of EEDP and the DREBF. The Nonlinear Static Analysis shown in Figure 31 reveals how adding the “Rehabilitation” system to the “Existing” system can create the target, rehabilitated, “Total” system. Adding the new REBF to the existing REBF created a combined system that worked in parallel to create the target system.

The NLTHA results in Figure 32 show that the “Rehabilitated” system clearly improved upon the “Existing” system. By adding the new REBF to the existing REBF, drift reduced by almost 50%, but only a 25% increase in base shear, as was desired. This again reveals the importance of considering the stiffness requirements along with strength requirements at the beginning of design.

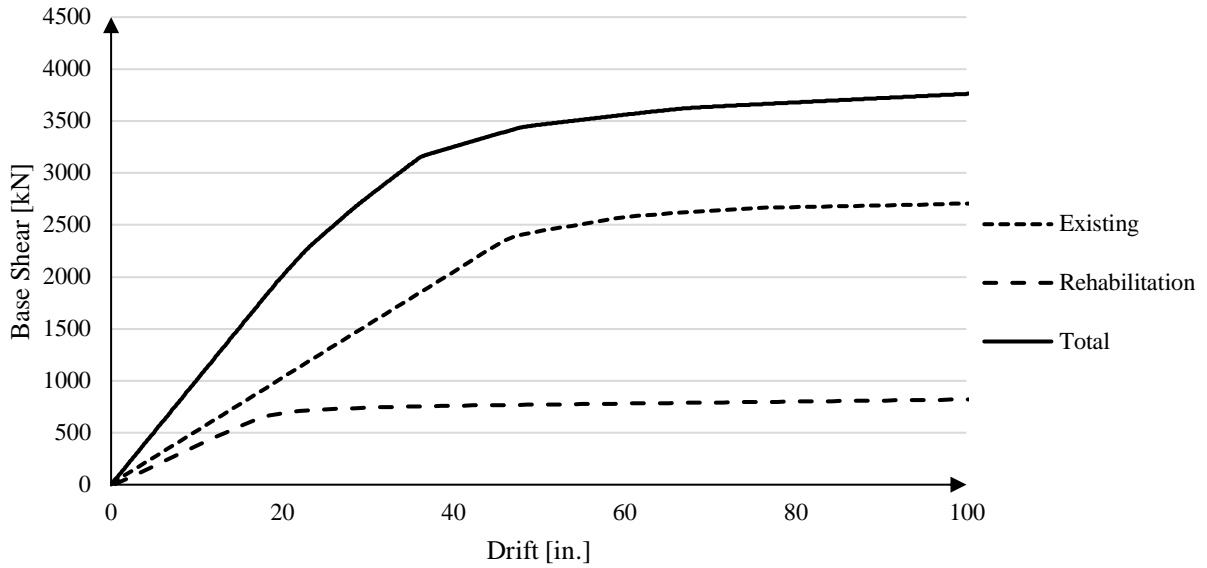


Figure 31. Pushover results from existing, rehabilitation and total systems

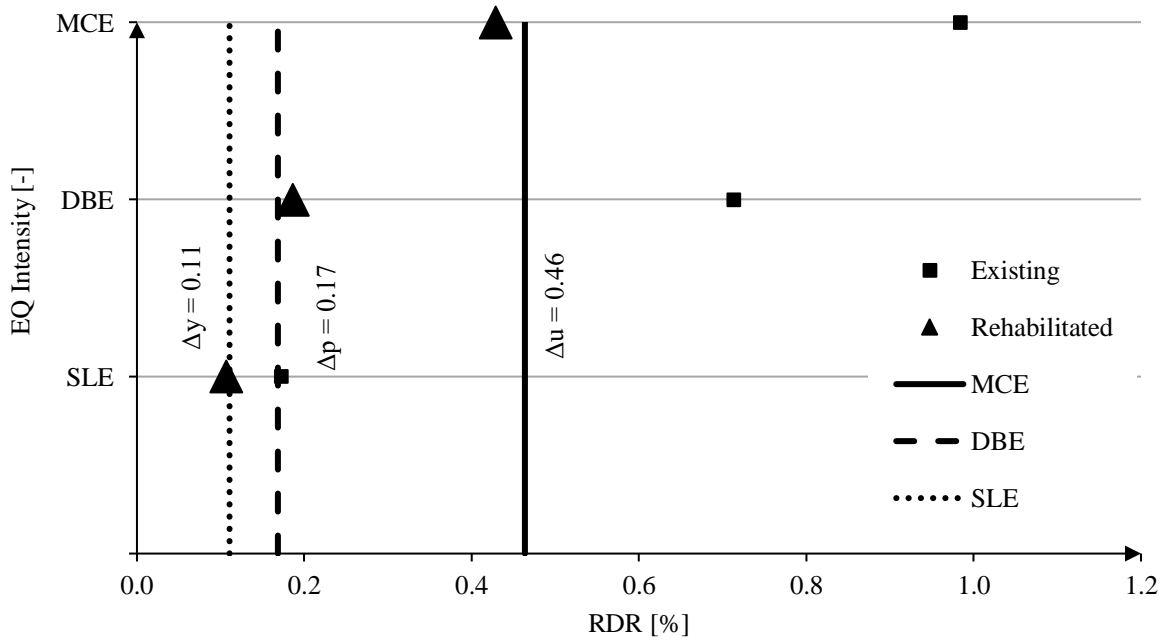


Figure 32. Median RDR Results of Existing and Rehabilitated systems

The findings of this experiment reveal that the use of EEDP is a reasonable option for design in a rehabilitation scenario.

Chapter 6: Summary and Conclusions

This chapter summarizes the findings and potential areas for further research. Section 6.1 presents an overall summary of the work accomplished, including the methodology used, results of numerical simulation and key findings in the performance evaluation of the DREBF under seismic load. Section 6.2 shows the potential areas for further research.

6.1 Summary

ESFP is a familiar and widely used design method by practicing structural engineers. ESFP offers many significant advantages, including ease of use and can be effectively programmed to a computer program. However, ESFP lacks clear consideration of the structural state after a strong earthquake shaking. Hence, it is not preferred for PBD. EEDP, on the other hand, is a powerful design methodology that uses the energy-balanced concept and plastic design procedure to design structures to achieve different performance objectives under different earthquake shaking intensities. It can be easily used by the designer in the office. In addition to the effectiveness of selecting the structures to achieve both the strength and stiffness limits without iteration, EEDP can be used to design the structure to have a specific dominant period. More importantly, EEDP can be used to design fuse structures such as the DREBF without considering the R_d and R_o factors. To compare the effectiveness of the EEDP with ESFP, a prototype five-story office building was designed using both the ESFP and EEDP approaches. Detailed numerical models were developed using OpenSees to simulate the nonlinear static and dynamic responses of the DREBF designed using ESFP and EEDP. The numerical models were calibrated using the experimental results. The comparison of the numerical and experimental results show that the proposed numerical model

can be used to simulate the force-deformation response of the shear link very well. NLTHAs were performed on the two numerical models using the ground motion selected and scaled to match the design spectrum of the prototype model. The result revealed that the ESFP design showed signs of yielding at the SLE hazard level, which reflected poorly on the seismic performance of the ESFP design. On the other hand, the EEDP design followed the pattern specified by the designer, where the primary system yielded at the DBE and secondary system yielded at the MCE hazard level. This shows that EEDP can control the damage state of the structure at different earthquake shaking intensities.

In addition to monitoring the drift and yielding patterns, the NLTHA results were also used in the PBEE evaluation. PBEE provided a clear presentation of a monetary quantification of the probable repair cost associated with the two models designed using ESFP and EEDP. The results of PBEE showed the probability of damage for the ESFP design was higher and costlier than that for the EEDP design.

EEDP was further explored for the use of rehabilitation. The prototype building presented in Chapter 2 was used as the existing building that needed to be rehabilitated. This building was assumed to have a single REBF frame as an existing SFRS which was identical to the secondary REBF designed in Chapter 2 using EEDP. The building needed to be rehabilitated to match the performance of the DREBF from Chapter 2. This was achieved by adding a rehabilitation system which was identical to the primary REBF shown in the EEDP design in Chapter 2. The combination of these two systems resulted in the same response as the DREBF presented in Chapter 2. The results of this exploration revealed how EEDP can be implemented in a backward manner and give reliable results.

6.2 Future Research Needs

Exploration in the use of EEDP as a conventional design procedure did reveal several intriguing areas where valuable research can be conducted. Suggested avenues of further exploration into EEDP and REBFs are summarized below:

- (i) This thesis focused on the use of EEDP to design a conventional building in Vancouver BC. The seismicity of this region was not used to develop EEDP and therefore, the empirical factors γ_a & γ_b , needed to be acquired. Thus it is suggested that, further research be required to determine more parameters for calculating these empirical energy transformation factors. A possible starting point may be to include the seismic hazard as well as the ductility and fundamental period of the building in the calculation of γ_a & γ_b .
- (ii) The REBF relied heavily on the stiffness and yield strength of the link to provide the desired bi-linear response. The possible bi-linear responses an REBF can give are limited by the stiffness and strengths of common W-shape sections. Further research could be carried out to determine how to manipulate these W-shape sections to give a wider range of stiffness and yield strength combinations.
- (iii) It was difficult to design a practical DREBF that achieved a large ductility (observed average $\Delta_p / \Delta_y = 1.55$) while satisfying the energy balance between the ELSDOF and ENLSDOF. Further exploration into how a larger ductility can be achieved using EEDP and the DREBF may expand the design flexibility of EEDP, allowing the DREBF to achieve a wider range of drift targets.
- (iv) Rehabilitation design can be achieved using EEDP. However, a limited example was shared in this study. Buildings owners who wish to rehabilitate their building, may desire a tri-linear

response of their rehabilitated structure that is not possible to achieve based on the ductility of the system and seismic hazard of the region. Further research could be made using EEDP as a rehabilitation design procedure, exclusively to highlight the constraints and flexibility of EEDP for buildings in need of rehabilitation in any seismic hazard.

Bibliography

- [1] K. J. Elwood, “Performance of concrete buildings in the 22 February 2011 Christchurch earthquake and implications for Canadian codes 1,” *NRC Res. Press*, vol. 776, no. February 2011, pp. 759–776, 2013.
- [2] National Research Council of Canada, “National Building Code of Canada 2015.” 2015.
- [3] M. J. N. Priestley, “Performance Based Seismic Design,” *12th WCEE*, vol. 1, no. 1, pp. 1–22, 2000.
- [4] G. W. Housner, “Limit Design of Structures to Resist Earthquakes,” *Calif. Inst. Technol.*, 1956.
- [5] A. Christopoulos, C., Filiatrault, *Principles of Passive Supplemental Damping and Seismic Isolation*. Multimedia Cardano, 2006.
- [6] H. Akiyama, “Earthquake-Resistant Limit-State Design for Buildings,” *Univ. Tokyo Press.*, no. Tokyo, 1985.
- [7] H. Akiyama, “Earthquake Resistant Design Based on the Energy Concept,” *9th World Conf. Earthq. Eng.*, no. Tokyo, Japan, 1988.
- [8] H. Akiyama, “Seismic Resistant Steel Structures: Method Based on Energy Criteria (Chapter 3),” *Int. Cent. Mech. Sci.*, no. Springer Verlag Wien, New York, 2000.
- [9] M. Fischinger, “Performance-Based Seismic Engineering: Vision for an Earthquake Resilient Society,” *Springer Dordr. Heidelb.*, no. New York, 2014.
- [10] S. C. Goel, “Performance-Based Plastic Design Of Earthquake Resistant Steel Structures (Design Guide),” 2007.
- [11] S. H. Chao, S. C. Goel, and S. S. Lee, “A seismic design lateral force distribution based on inelastic state of structures,” *Earthq. Spectra*, vol. 23, no. 3, pp. 547–569, 2007.

- [12] S. Chao, M. R. Bayat, and S. C. Goel, “Performance-Based Plastic Design Of Steel Concentric Braced Frames For Enhanced Confidence Level,” in *14th WCEE*, 2008.
- [13] W. Liao, M. R. Bayat, and S. Chao, “Performance-Based Plastic Design (PBPD) Method For Earthquake-Resistant Structures : An Overview,” *Struct. Des. Tall Spec. Build.*, vol. 137, no. October 2009, pp. 115–137, 2010.
- [14] N. Newmark and W. Hall, “‘Earthquake Spectra and Design,’ Engineering Monographs on Earthquake Criteria, Structural Design, and Strong Motion Records,” *Earthq. Eng. Res. Institute, Univ. Calif. , Berkeley, CA.*, vol. 3, 1982.
- [15] M. Bosco, E. M. Marino, and P. P. Rossi, “Modelling Of Steel Link Beams Of Short, Intermediate Or Long Length,” *Eng. Struct.*, vol. 84, pp. 406–418, 2015.
- [16] Y. Shen, C. Christopoulos, M. Asce, N. Mansour, and R. Tremblay, “Seismic Design and Performance of Steel Moment-Resisting Frames with Nonlinear Replaceable Links,” *J. Struct. Eng.*, vol. 137, no. October, pp. 1107–1117, 2011.
- [17] J. W. Berman, T. Okazaki, and H. O. Hauksdottir, “Reduced Link Sections for Improving the Ductility of Eccentrically Braced Frame Link-to-Column Connections,” *J. Struct. Eng.*, no. May, 2010.
- [18] A. Daneshmand and B. Hosseini, “Performance of intermediate and long links in eccentrically braced frames,” *JCSR*, vol. 70, pp. 167–176, 2012.
- [19] M. R. Esmaili, “Seismic Performance of Eccentrically Braced Frames Designed According to Canadian Seismic Provisions School of Graduate Studies,” no. May, 2015.
- [20] G. S. Prinz and P. W. Richards, “Eccentrically braced frame links with reduced web sections,” *J. Constr. Steel Res.*, vol. 65, no. 10–11, pp. 1971–1978, 2009.
- [21] M. Bruneau, C. Uang, and R. Sabelli, *Ductile Design of Steel Structures*. .

- [22] G. C. Clifton, C. K. Seal, and G. A. Macrae, "Performance of Eccentrically Braced Framed Buildings In The Christchurch Earthquake Series of 2010 / 2011," in *15th World Conference on Earthquake Engineering*, 2012, no. November 2015.
- [23] P. Dusicka and J. W. Berman, "Steel Frame Lateral System Concept Utilizing Replaceable Links," *2009 NZSEE Conf. Abstr.*, 2009.
- [24] P. Dusicka, "Investigation of Replaceable Sacrificial Steel Links," 2009.
- [25] C. Zhao and K. Gong, "Finite Element Analysis of the Seismic Behaviors on Web-Bolted Connected of Replaceable Shear Links for Eccentrically Braced Steel Frame," *Adv. Mater. Res.*, vol. 1020, pp. 258–263, 2014.
- [26] N. Mansour, "Development of the Design of Eccentrically Braced Frames with Replaceable Shear Links," University of British Columbia, 2010.
- [27] Canadian Standards Association, *S16-14*. Mississauga, Ontario: CSA Group, 2014.
- [28] D. Dimakogianni, G. Dougka, I. Vayas, and P. Karydakis, "Seismic Behaviour Of Innovative Energy Dissipation Systems Fuseis 1-2," in *4th ECCOMAS Thematic Conference*, 2013.
- [29] P. Dusicka and R. Iwai, "Development of Linked Column Frame System for Seismic Lateral Loads."
- [30] A. P. Lopes and P. Dusicka, "Design of the Linked Column Frame Structural System," 2007.
- [31] P. Hsiao, K. Hayashi, H. Inamasu, and Y. Luo, "Development and Testing of Naturally Buckling Steel Braces," *J. Struct. Eng.*, vol. 142, no. 1, 2016.
- [32] M. Malakoutian, J. W. Berman, and P. Dusicka, "Seismic Response Evaluation Of The Linked Column Frame System," pp. 1–39.

- [33] T. Y. Yang, Y. Li, S. C. Goel, and M. Asce, “Seismic Performance Evaluation of Long-Span Conventional Moment Frames and Buckling-Restrained Knee-Braced Truss Moment Frames,” *J. Struct. Eng.*, vol. 4015081, no. 14, 2016.
- [34] T. Y. Yang, D. P. Tung, and Y. Li, “Equivalent energy-based design procedure for innovative earthquake resilient structures,” *Earthq. Eng. Struct. Dyn. (under Rev.)*, 2016.
- [35] T. Y. Yang, D. P. Tung, and Y. Li, “Equivalent Energy Design Procedure for Innovative Earthquake Resilient Structures – Theory,” 2010.
- [36] T. Y. Yang, D. P. Tung, and Y. Li, “Equivalent Energy Design Procedure for Innovative Earthquake Resilient Structures – Application,” pp. 1–23, 2011.
- [37] M. Murphy, “Performance Based Evaluation Of Prequalified Steel Seismic Force Resisting Structures In Canada,” 2012.
- [38] American Society of Civil Engineering, “Seismic provisions for structural steel buildings ANSI/AISC 341-10,” *American Institute of Steel Construction, Chicago, IL., USA*. 2010.
- [39] ANSI/AISC 360-10, “Specification for Structural Steel Buildings,” *American Institute of Steel Construction, Chicago, IL., USA*. 2010.
- [40] PEER, “Next Generation Attenuation Ground Motion Database,” *Pacific Earthquake Engineering Research Center*, 2010. [Online]. Available: ngawest2.berkeley.edu.
- [41] Applied Technology Council, “Seismic Performance Assessment of Buildings FEMA P58,” 2012.
- [42] L. Mastrandrea, “Plastic Design of Eccentrically Braced Frames , II : Failure Mode Control Plastic design of eccentrically braced frames , II : Failure mode control,” *J. Constr. Steel Res.*, vol. 65, no. 5, pp. 1015–1028, 2009.
- [43] L. Mastrandrea, E. Nastri, and V. Piluso, “Validation of a Design Procedure for Failure

- Mode Control of EB-Frames : Push-Over and IDA Analyses,” *Open Constr. Build. Technol. J.*, pp. 193–207, 2013.
- [44] T. Y. Yang, “Performance Evaluation of Innovative Steel Braced Frames,” Universtiy of California, Berkley, 2006.
- [45] H. Varum, F. Teixeira-Dias, P. Marques, A. V. Pinto, and A. Q. Bhatti, “Performance Evaluation Of Retrofitting Strategies For Non-Seismically Designed RC Buildings Using Steel Braces,” *Bull Earthq. Eng.*, vol. 11, pp. 1129–1156, 2013.
- [46] American Society of Civil Engineering, “Seismic Rehabilitation of Existing Buildings ASCE/SEI 41-13,” 2014.

Appendix A: Site & Building Description

The site and building definition are given more detail in this section. The 5-storey office building is in Vancouver BC, Canada and the loads are directly taken from Michael Murphy's [37] prototype building. Load calculation is based on NBCC 2010 load combination 1.0D + 1.0E + 0.25S. The dead load includes self-weight of primary and secondary framing members as well as flooring, mechanical electrical and plumbing, and superimposed dead load. The snow load is calculated based on the standard code formula and precipitation factors provided by the code for the Vancouver region. The tributary gravity loads applied to the frame are based on the same formulation and a tributary width of a half bay – gravity loads were applied during all simulations.

Seismic Weight Distribution for Model

| Level | DL [kN] | 25%SL [kN] | Total [kN] |
|---------------------|---------|------------|--------------|
| Roof | 5868 | 1418 | 7286 |
| 5th | 11850 | - | 11850 |
| 4th | 11850 | - | 11850 |
| 3rd | 11850 | - | 11850 |
| 2nd | 11850 | - | 11850 |
| Total W (kN) | = | | 54687 |

Geometry and Tributary Loads Applied to Model

| Floor | hx [m] | hx [in.] |
|---------------------------------|---------------|------------------|
| 5 | 18.85 | 742.13 |
| 4 | 15.2 | 598.43 |
| 3 | 11.55 | 454.72 |
| 2 | 7.9 | 311.02 |
| 1 | 4.25 | 167.32 |
| Bay Width (m , in) | 9 | 354.3 |
| Beam Length (0.61m link) | 4.20 | 165.17 |
| Trib. Gravity Frame Load | [kN/m] | [kip/in.] |
| Roof | 12.6 | 0.072 |
| Floor | 22.86 | 0.131 |

The building is located on site class C soil, the spectrum is defined by the following table as defined by NBCC 2015:

| Period | Site | Foundation |
|--------|-----------|------------|
| T [s] | Sa(T) [g] | F(T) |
| 0 | 0.841 | 1 |
| 0.2 | 0.841 | 1 |
| 0.5 | 0.748 | 1 |
| 0.8 | 0.553 | 1 |
| 1 | 0.422 | 1 |
| 2 | 0.255 | 1 |
| 5 | 0.081 | 1 |

Appendix B: Equivalent Static Force Procedure

The base shear calculated using ESFP is comprehensively displayed in this section. The calculation (linear interpolation) for spectral acceleration is given and the table below shows the parameters used.

$$S_a(0.71) = 0.748 - 0.748 - (0.748 - 0.553) * \frac{(0.71 - 0.5)}{(0.8 - 0.5)} = 0.6115g$$

| Building Category | Normal | Notes |
|-------------------|----------|----------------|
| Ie | 1 | |
| Rd | 4 | |
| Ro | 1.5 | |
| hn (m) | 18.85 | |
| Model Period (s) | 0.71 | Modal Analysis |
| Tn=0.025*hn (s) | 0.47 | |
| Design Period | 0.71 | |
| Site Class C | F(T) = 1 | Table 4.1.8.4 |
| Sa(0.2)/Sa(2.0) | 3.30 | Table 4.1.8.11 |
| Mv | 1 | |
| J | 1 | |
| S(Ta) (g)= | 0.6115 | |

$$\text{Lower Limit: } V_e = \frac{S(2.0)M_v I_E W}{R_d R_o} = \frac{0.255 * 1.0 * 1.0 * 54687}{4 * 1.5} = 2324 \text{ kN}$$

$$\text{Upper Limit 1: } V_e = \frac{2S(0.2)I_E W}{3R_d R_o} = \frac{2 * 0.841 * 1.0 * 54687}{3 * 4 * 1.5} = 5110 \text{ kN}$$

$$\text{Upper Limit 2: } V_e = \frac{S(0.5)I_E W}{R_d R_o} = \frac{0.748 * 1.0 * 54687}{4 * 1.5} = 6818 \text{ kN}$$

$$\text{Elastic Base Shear: } V_e = \frac{S(T_a)M_v I_E W}{R_d R_o} = \frac{0.6115 * 1.0 * 1.0 * 54687}{4 * 1.5} = 5574 \text{ kN}$$

$$\text{Design with accidental torsion} = 1.1 * V_e, \quad V_d = 6131 \text{ kN}$$

$$\text{Whipping Effect: } F_t = \min(0.25 * V_d, 0.07 * T * V_d) = 305 \text{ kN}$$

The calculated loads need to be distributed up the building as floor shears and are done so per the formula:

$$F_x = (V - F_t) \frac{W_x h_x}{\sum_{i=1}^n W_i h_i}$$

Load Distribution

| Level | W _x [kN] | h _x [m] | W _x *h _x [kN-m] | F _x [kN] | F _x per frame [F _x /4, kN] | F _x per node [F _x /8, kN] | nodal mass [kg] | nodal mass [kip*s ² /in] |
|--------------|---------------------|--------------------|---------------------------------------|---------------------|--|---|-----------------|-------------------------------------|
| Roof | 7286 | 18.85 | 137340 | 1642 | 411 | 205 | 92933 | 0.531 |
| 5th | 11850 | 15.2 | 180125 | 1754 | 438 | 219 | 151152 | 0.863 |
| 4th | 11850 | 11.55 | 136871 | 1333 | 333 | 167 | 151152 | 0.863 |
| 3rd | 11850 | 7.9 | 93617 | 912 | 228 | 114 | 151152 | 0.863 |
| 2nd | 11850 | 4.25 | 50364 | 490 | 123 | 61 | 151152 | 0.863 |
| Total | 54687 | | 598317 | 6131 | 1533 | 766 | | |

Load Transformation

| Level | V _i [kN] | h [m] | V _u = V _i *h/L [kN] | Section | GA [N] | M _p [kN-m] | V _p [kN] | e [m] | Link resistance [kN] | V _{link} Probable [kN] |
|-------|---------------------|-------|---|----------------|-----------|-----------------------|---------------------|-------|----------------------|---------------------------------|
| Roof | 411 | 3.65 | 166 | W150x18 | 68329800 | 47 | 168 | 0.31 | 139 | 169 |
| 5th | 849 | 3.65 | 344 | W310x28 | 142758000 | 140 | 352 | 0.61 | 317 | 386 |
| 4th | 1182 | 3.65 | 479 | W310x67 | 200277000 | 362 | 494 | 0.61 | 444 | 542 |
| 3rd | 1410 | 3.65 | 572 | W310x107 | 261022300 | 611 | 643 | 0.61 | 579 | 706 |
| 2nd | 1533 | 4.25 | 724 | W310x129 | 320766600 | 745 | 790 | 0.61 | 711 | 868 |

To calculate link expected resistances, S16-09 [27] gives the following formulas to follow, the expected values were increased by a factor of 1.22 to match the calibration to the data provided by Dusicka [30] which replaces the R_y and R_o factors of 1.3 and 1.1 respectively given by S16-09 to calculate the probable ultimate strength of the member:

$$V_p = 0.55AF_y$$
$$V_y = \text{Max}(\varphi_s V_p, \frac{2\varphi_s M_p}{e})$$
$$V_{pr} = 1.22V_y$$
$$M_p = \varphi_s Z F_y$$

As discussed in the body sections of this paper, the probable link force was then used to capacity design the members outside of the link. The values that were assigned to the capacity design half-bay model equal the plastic moment capacity, M_p and probable link resistance, V_{pr} .

Appendix B: Equivalent Energy Design Procedure

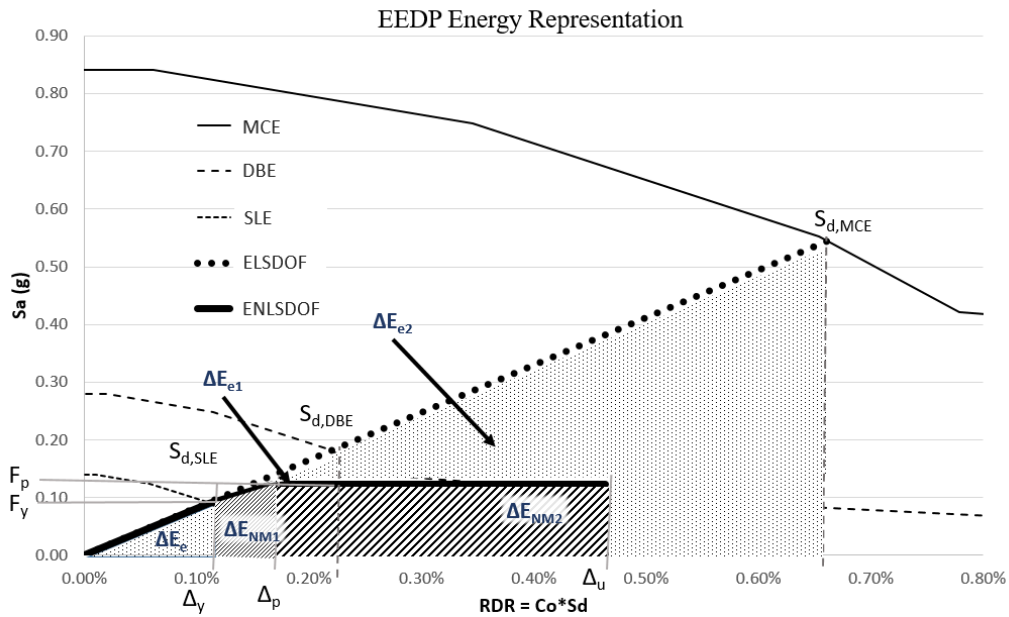
The base shears calculated using EEDP is comprehensively displayed in this section. The spectra (scaled from 2% in 50-year hazard in Vancouver, given in previous section, denoted “VAN”) used for design are given in the following table (MCE = 1.0*VAN, DBE = 0.333*VAN, SLE = 0.167 *VAN). The acceleration spectra are transformed into displacement spectra (given as roof drift ratios in percent) by the following formula, where C_o is the SDOF – MDOF transformation factor given by ASCE 14 [46]:

$$S_d = C_o * S_a \left(\frac{T}{2\pi} \right)^2$$

EEDP Design Spectra

| T | Sa (MCE) | Sd (MCE) | Sa (DBE) | Sd (DBE) | Sa (SLE) | Sd (SLE) |
|-------------|--------------|---------------|--------------|---------------|--------------|---------------|
| 0.05 | 0.841 | 0.004% | 0.280 | 0.001% | 0.140 | 0.001% |
| 0.2 | 0.841 | 0.062% | 0.280 | 0.021% | 0.140 | 0.010% |
| 0.5 | 0.748 | 0.345% | 0.249 | 0.115% | 0.125 | 0.058% |
| 0.8 | 0.553 | 0.653% | 0.184 | 0.218% | 0.092 | 0.109% |
| 1 | 0.422 | 0.779% | 0.141 | 0.259% | 0.070 | 0.130% |
| 2 | 0.255 | 1.883% | 0.085 | 0.627% | 0.043 | 0.315% |
| 5 | 0.081 | 3.739% | 0.027 | 1.245% | 0.014 | 0.624% |
| 0.81 | 0.545 | 0.661% | 0.181 | 0.220% | 0.091 | 0.110% |

EEDP delivers a backbone that is defined as shown in the following figure, as referenced in the main body.



As per performance based design, the input objectives must be chosen (hence the above spectra). With EEDP, the first point of yield is chosen and the period and corresponding spectral acceleration are calculated:

For $\Delta_y = 21\text{mm}$ (0.11%)

$$(S_a)_{SLE} = 0.091g \text{ (Interpolation)}$$

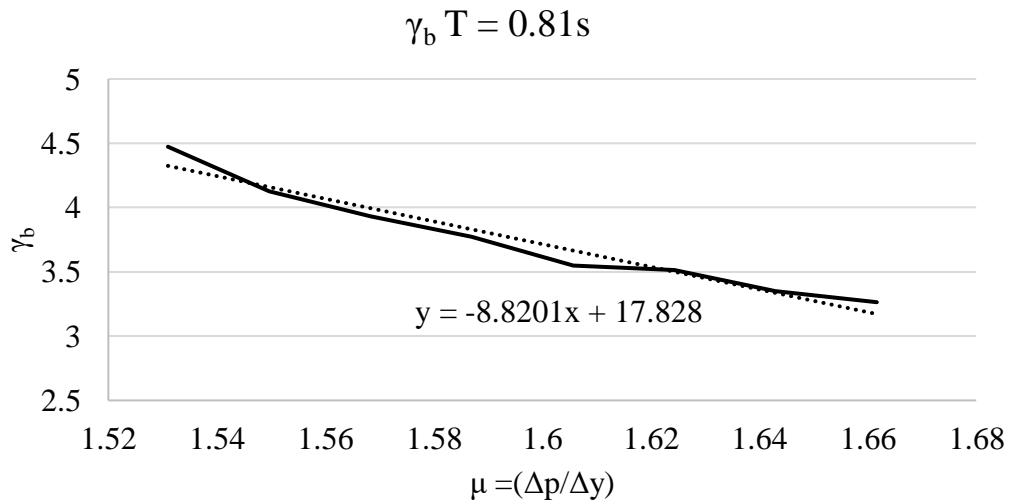
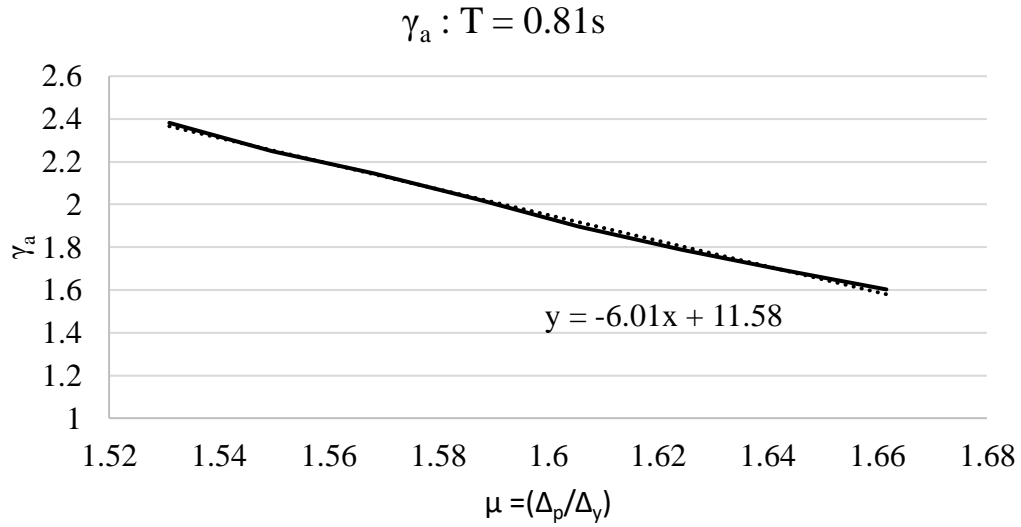
$$F_y = m(S_a)_{SLE} = 2482\text{kN}$$

$$T = 2\pi \sqrt{\frac{C_o S_d}{S_a}} = 2\pi \sqrt{\frac{1.4 * 0.0011}{0.091}} = 0.81\text{s}$$

$$\text{Elastic Energy at yield: } e_{SLE} = F_y * \Delta_y / 2 = 2482 * 0.021 / 2 = 26 \text{ kN.m}$$

For the second yield point, Δ_p , a displacement of 32mm was chosen. At this point it is crucial to calculate the energy values of each state, plus define the energy transformation factors:

$$\mu_p (\Delta_p / \Delta_y) = 32 / 21 = 1.52$$



Extrapolation $\gamma(\mu_p)$: $\gamma_a = 2.42$ & $\gamma_b = 4.4$

Elastic Energy at DBE level: $e_{DBE} = F_{DBE} * S_{d,DBE} / 2 = 4960 * 0.041 / 2 = 102 \text{ kN.m}$

Change in elastic energy to inelastic: $\Delta E_{NM1} = (e_{DBE} - e_{SLE}) / \gamma_a = (102 - 26) / 2.42 = 31.4 \text{ kN.m}$

Inelastic design force at Δ_p : $F_P = \frac{2\Delta E_{NM1}}{(\Delta_p - \Delta_y)} - F_y = \frac{2 * 31.4}{(0.032 - 0.021)} - 2482 = 3367 \text{ kN}$

Strength ratio: $\lambda = F_P / F_y = 3367 / 2482 = 1.36$

The final calculations for the design are to predict the ultimate roof drift which the MCE earthquake can push the building, Δ_u :

$$\text{Elastic Energy at MCE level: } e_{\text{MCE}} = F_{\text{MCE}} * S_{\text{d,MCE}} / 2 = 14896 * 0.125 / 2 = 931 \text{ kN.m}$$

$$\text{Change in elastic energy to inelastic: } \Delta E_{\text{NM2}} = (e_{\text{MCE}} - e_{\text{DBE}}) / \gamma_b = (931 - 102) / 4.04 = 195 \text{ kN.m}$$

$$\text{Design max roof drift: } \Delta_u = (\Delta E_{\text{NM2}} / F_p) + \Delta_p = (195 / 3367) + 0.032 = 90 \text{ mm}$$

With the backbone defined, the next step is to separate the tri-linear action into two distinct bi-linear systems that work in parallel.

$$\text{Primary Bi-linear system: } F_{\text{PR}} = F_y \frac{\mu_p^{-\lambda}}{\mu_p^{-1}} = 2482 * \frac{1.52^{-1.36}}{1.52^{-1}} = 782 \text{ kN}$$

$$\text{Secondary Bi-linear system: } F_{\text{SE}} = F_y \mu_p \frac{\lambda-1}{\mu_p^{-1}} = 2482 * 1.52 * \frac{1.36-1}{1.52^{-1}} = 2584 \text{ kN}$$

With The primary and secondary base shears defined, the base shears need to be distributed up the building as storey shears, where then they are transformed to link shear demands. The primary system distribution is shown in the following steps; the secondary is follows the same pattern but is not shown.

$$\text{Factor defined by Goel and Chao [13]: } \beta_i = \left(\frac{\sum_{j=1}^n w_j h_j}{w_n h_n} \right)^{0.75T^{-0.2}}$$

$$\text{Factor defined by Goel and Chao [13]: } C_{vi} = (\beta_i - \beta_{i+1}) \left(\frac{w_n h_n}{\sum_{j=1}^n w_j h_j} \right)^{0.75T^{-0.2}}$$

$$\text{Storey Shear at level 'i': } F_{\text{pri}} = C_{vi} F_{\text{pr}}$$

With the storey shears defined, the kinematic method is used to define how the storey shears are resisted by the link.

$$W_{ext} = \sum F_{pri} \Delta_i; \Delta_i = \theta_p H_i$$

$$W_{int} = \sum V_{link,i} \delta; \delta = L \theta_p \therefore = \sum \beta_i V_{link,roof} L \theta_p$$

$$W_{ext} = W_{int} \therefore V_{link,roof} = \frac{\sum F_{pri} H_i}{\sum \beta_i L}$$

$$V_i = V_{link,roof} \beta$$

Lateral force distributed vertically

| Floor | hx (m) | Wi (kN) | wihi | β_i | C'vi | Fpri (kN) | FpriHi | Vi (kN) |
|-------|--------|----------|-------|-----------|-------|-----------|--------------|---------|
| Roof | 18.85 | 3642.975 | 68670 | 1 | 0.316 | 248 | 4666 | 105 |
| 4 | 15.2 | 5925.15 | 90062 | 1.93 | 0.293 | 229 | 3482 | 202 |
| 3 | 11.55 | 5925.15 | 68435 | 2.55 | 0.197 | 154 | 1781 | 267 |
| 2 | 7.9 | 5925.15 | 46809 | 2.95 | 0.127 | 99 | 786 | 309 |
| 1 | 4.25 | 5925.15 | 25182 | 3.16 | 0.066 | 52 | 221 | 331 |
| | | | | | | | Vroof | 105 |

Sizing the links to the demand followed the same pattern as given by the ESFP, except the probable shear strength was used for sizing as opposed to the yield strength.

$$V_{design} = V_{pr} = 1.22 * 0.55 A F_y$$

| Level | Vpri (kN) | Section | Vpr.(kN) | Mp.(kNm) |
|-------|-----------|---------|----------|----------|
| Roof | 105 | W100x19 | 174 | 53 |
| 5th | 202 | W150x18 | 205 | 63 |
| 4th | 267 | W200x22 | 296 | 90 |
| 3rd | 309 | W200x31 | 311 | 95 |
| 2nd | 331 | W200x42 | 342 | 104 |

| Level | Vsei (kN) | Section | Vpr.(kN) | Mp.(kNm) |
|-------|-----------|----------|----------|----------|
| Roof | 347 | W200x42 | 342 | 104 |
| 5th | 668 | W310x74 | 675 | 206 |
| 4th | 884 | W310x129 | 964 | 294 |
| 3rd | 1023 | W310x143 | 1047 | 319 |
| 2nd | 1096 | W310x158 | 1173 | 358 |

Capacity design is then carried out with SAP using the design shears and corresponding moment capacities as discussed in the body of this paper. The loads inputted into the model given below and defined by the force restoration formulas defined by Goel and Chao [13].

$$\text{Restoring force: } F_{right} = \frac{\sum_i^n (M_{pi} + L_b V_{pri} - \frac{L_b w_i^2}{2})}{\sum_i^n C_{vi} h_i}$$

$$\text{Restoring force: } F_{left} = \frac{\sum_i^n (M_{pi} + L_b V_{pri} + \frac{L_b w_i^2}{2})}{\sum_i^n C_{vi} h_i}$$

$$\text{Storey restoring force: } F_{i,right} = C_{vi} F_{right}$$

$$\text{Storey restoring force: } F_{i,left} = C_{vi} F_{left}$$

| h (m) | Cvi | Gravity (kN.m) | Vp (kN) | Mp (kN.m) | Fi Right (kN) | Fi Left (kN) |
|-------|-------|----------------|---------|--------------|---------------|--------------|
| 18.85 | 0.316 | 8676 | 174 | 4155 | 115 | -156 |
| 15.2 | 0.293 | 15740 | 205 | 4899 | 106 | -144 |
| 11.55 | 0.197 | 15740 | 296 | 7051 | 71 | -97 |
| 7.9 | 0.127 | 15740 | 311 | 7420 | 46 | -63 |
| 4.25 | 0.066 | 15740 | 342 | 8149 | 24 | -33 |
| | | Fr Right (kN) | 362 | Fr Left (kN) | 493 | |

The materials and sections were defined in OpenSEES TCL script for the primary system as follows, note that the same procedure was also used for the ESFP model as well:

| Fibre Bending Material | | | | | | | | | | | | |
|---------------------------|------------|----------|-----------|--------|----------|-------------|------|-------|----|-------|-----|--------|
| Material | matTag | Fy | E | b | R0 | cR1 | cR2 | <a1 | a2 | a3 | a4> | <sig0> |
| Steel02 | 2 | 50.8 | 29000 | 0.05 | 18.5 | 0.925 | 0.15 | 0 | 1 | 0 | 1 | 0 |
| Shear Aggregator Material | | | | | | | | | | | | |
| Material | matTag | Fy | E | b | R0 | cR1 | cR2 | <a1 | a2 | a3 | a4> | <sig0> |
| Steel02 | 10 | 39.17 | 13024.33 | 0.003 | 18.5 | 0.925 | 0.15 | 0.033 | 1 | 0.033 | 1 | 0 |
| Steel02 | 12 | 46.18 | 15357.15 | 0.003 | 18.5 | 0.925 | 0.15 | 0.033 | 1 | 0.033 | 1 | 0 |
| Steel02 | 14 | 66.47 | 22102.95 | 0.003 | 18.5 | 0.925 | 0.15 | 0.033 | 1 | 0.033 | 1 | 0 |
| Steel02 | 16 | 69.95 | 23258.97 | 0.003 | 18.5 | 0.925 | 0.15 | 0.033 | 1 | 0.033 | 1 | 0 |
| Steel02 | 18 | 76.82 | 25543.34 | 0.003 | 18.5 | 0.925 | 0.15 | 0.033 | 1 | 0.033 | 1 | 0 |
| Section Aggregator | | | | | | | | | | | | |
| | Aggregator | \$secTag | \$matTag1 | \$dof1 | | section tag | | | | | | |
| section | Aggregator | 800 | 10 | Vy | -section | 84 | | | | | | |
| section | Aggregator | 802 | 12 | Vy | -section | 87 | | | | | | |
| section | Aggregator | 804 | 14 | Vy | -section | 95 | | | | | | |
| section | Aggregator | 806 | 16 | Vy | -section | 97 | | | | | | |
| section | Aggregator | 808 | 18 | Vy | -section | 99 | | | | | | |

In addition to the results given in Chapter 5 of this paper, the following table also tabulates results from the NLTHA.

| MCE | Base Shear (kip) | | | Interstorey Drift (%) | | Roof Displacement (in) | | | RDR (%) | | Roof Acc. (g) | |
|------|------------------|------|---------|-----------------------|---------|------------------------|------|--------|---------|--------|---------------|---------|
| | Target | Max | Average | Max | Average | Target | Max | Median | Max | Median | Max | Average |
| EEDP | 757 | 1395 | 1070 | 1.10 | 0.71 | 3.44 | 5.20 | 3.18 | 0.70 | 0.43 | 1.14 | 0.67 |
| ESFP | 689 | 1314 | 1082 | 0.89 | 0.70 | 18.55 | 5.54 | 3.25 | 0.75 | 0.44 | 1.06 | 0.66 |
| | | | | | | | | | | | | |
| DBE | Base Shear (kip) | | | Interstorey Drift (%) | | Roof Displacement (in) | | | RDR (%) | | Roof Acc. (g) | |
| | Target | Max | Average | Max | Average | Target | Max | Median | Max | Median | Max | Average |
| EEDP | 757 | 803 | 746 | 0.30 | 0.23 | 1.25 | 1.60 | 1.38 | 0.22 | 0.19 | 0.52 | 0.36 |
| ESFP | - | 895 | 828 | 0.41 | 0.28 | - | 1.56 | 1.27 | 0.21 | 0.17 | 0.46 | 0.34 |
| | | | | | | | | | | | | |
| SLE | Base Shear (kip) | | | Interstorey Drift (%) | | Roof Displacement (in) | | | RDR (%) | | Roof Acc. (g) | |
| | Target | Max | Average | Max | Average | Target | Max | Median | Max | Median | Max | Average |
| EEDP | 558 | 680 | 529 | 0.18 | 0.14 | 0.82 | 1.13 | 0.79 | 0.15 | 0.11 | 0.36 | 0.23 |
| ESFP | - | 803 | 606 | 0.22 | 0.15 | - | 1.20 | 0.69 | 0.16 | 0.09 | 0.29 | 0.24 |

Appendix D: Rehab Calculations

This portion of appendix describes the process used to apply EEDP for the sake of rehabilitation. The implementation follows the same principles as if designing for a new build, except in this manner, the “softer” bi-linear system is already defined as the existing SFRS. Back calculation is required to define the response of the rehabilitation system to be added to the existing structure. It is assumed that specific consultation with the owner is carried out to define how the building is desired to respond. The following describes the steps taken to size the new system for the existing structure described in Chapter 6.

Step 1. Define the response of the existing system

A pushover model is built in OpenSEES that replicates the frame of the existing SFRS using on the secondary frame. The response gave similar values to the design values which were a yield drift and strength of the existing system as 33mm (1.3”) and 2600kN (585kip) respectively.

Step 2. Define the response of the desired system

The serviceability drift and ultimate base shear strength are desired as 20mm (0.8”) and 3390kN (760kip) respectively. With this information, the trilinear backbone curve is defined with the added rehabilitation system and existing system that will be working in parallel. The target is described in Figure 18, where the tri-linear curve is the rehabilitated system, PR is the added system and SE is the existing. Note that the yield strength is calculated as the sum of the yield strength of the rehabilitated system plus the elastic force incurred by the existing system at the desired yield drift, which in this case is 2440kN (548kip).

The same parameters from table 5 are used to design and size the links of the system, which follows the same kinematic process as discussed for EEDP in the previous section.

Step 3. Define characteristics of the rehabilitation system

The period of the existing system will be adjusted due to the new system and is defined using the same functions as described earlier.

- Existing system period: $T = 2\pi \sqrt{\frac{m \Delta_y}{C_o F_y}} = 2\pi \sqrt{\frac{15.91 * 1.3}{1.4 * 585}} = 0.99s$, OpenSEES: 1.06s
- Rehabilitated system: $T = 2\pi \sqrt{\frac{m \Delta_y}{C_o F_y}} = 2\pi \sqrt{\frac{15.91 * 0.8}{1.4 * 548}} = 0.81s$, OpenSEES: 0.75s

Step 4. Define design spectra

The design spectra are assumed to be derived from the 2% in 50yr UHS for Vancouver, taken as MCE and SLE is defined by the desired yield drift and corresponding base shear which is transformed into a spectral acceleration:

$$\text{Spectral acceleration at first yield: } S_a = F_y/mg = 548/(15.91 * 386.4) = 0.09g = 16\% \text{ UHS}$$

$$\text{Elastic energy at first yield: } e_{SLE} = F_y * \Delta_y / 2 = 548 * 0.8 / 2 = 222 \text{ kip.in}$$

As discussed in the main body of this paper, the DBE response relies on the inelastic behaviour of the yielded primary system.

$$\Delta E_{NMI} = (F_y + F_p) * (\Delta_p - \Delta_y) / 2, \Delta E_{NMI} = (548 + 760) * (1.3 - 0.8) / 2 = 310 \text{ kip.in}$$

Back calculating the elastic energy e_{DBE} :

- $e_{DBE} = \Delta E_{NMI} * \gamma_a + e_{SLE} = 310 * 2.07 + 222 = 860 \text{ kip.in}$

- $e_{DBE} = mg S_{aDBE} * g S_{dDBE} / 2,$

$$\text{where } S_{dDBE} = S_{aDBE} C_o (T/2\pi)^2$$

- Solve: $S_{aDBE} = \sqrt{\frac{2 e_{DBE}}{m g^2 C_o \left(\frac{T}{2\pi}\right)^2}} = \sqrt{\frac{2 * 860}{15.91 * 386.4 * 386.4 * 1.4 * \left(\frac{0.81}{2\pi}\right)^2}} = 0.18g = 33\% \text{ UHS}$

- Corresponding roof drift = $g * S_{dDBE} = 386.4 * 0.18 * 1.4 * (0.81/2\pi)^2 = 1.6 \text{ in} > \Delta_p$

These results indicate the complexity involved with solving multi-variable problem.

The MCE response relies on the behaviour of the SFRS with both the primary and secondary fuses yielded. In this case the UHS for Vancouver is used as mentioned. From this level of shaking and γ_b values taken from table 5, the ultimate roof drift, Δ_u is estimated.

$$- \Delta E_{NM2} = (e_{MCE} - e_{DBE}) / \gamma_b$$

$$\text{Where } e_{MCE} = mgS_{aMCE} * gS_{dMCE} / 2 = 15.91 * 386.4 * 0.546 * 386.4 * 0.0127 / 2 = 8251 \text{ kip.in}$$

$$\Delta E_{NM2} = (8251 - 860) / 3.89 = 1900 \text{ kip.in}$$

$$\text{Max drift} = \Delta u = \Delta E_{NM2} / F_p + \Delta_p = 1900 / 760 + 1.3 = 3.8 \text{ in (RDR} = 3.8 / 742 = 0.5\%)$$

The figure below summarizes the results from the design spectra analysis. This is the design behaviour of the SFRS:

| VAN UHS Definition | MCE | DBE | SLE |
|--------------------|-----------|-----------|-----------|
| Period | Site | Site | Site |
| T (s) | Sa(T) (g) | Sa(T) (g) | Sa(T) (g) |
| 0.005 | 0.841 | 0.271 | 0.137 |
| 0.2 | 0.841 | 0.271 | 0.137 |
| 0.50 | 0.748 | 0.241 | 0.122 |
| 0.8 | 0.553 | 0.178 | 0.090 |
| 1 | 0.422 | 0.136 | 0.069 |
| 2 | 0.255 | 0.082 | 0.042 |
| 5 | 0.081 | 0.026 | 0.013 |
| 0.81 | 0.546 | 0.176 | 0.089 |
| Sd @ period (in) | 4.913 | 1.586 | 0.801 |

